

# UC Berkeley

## UC Berkeley Electronic Theses and Dissertations

### Title

The Effects of Obesity on Murine Cortical Bone

### Permalink

<https://escholarship.org/uc/item/7cm8m2r5>

### Author

Martin, Sophi

### Publication Date

2010

Peer reviewed|Thesis/dissertation

The Effects of Obesity on Murine Cortical Bone

by

Sophi Martin

A dissertation submitted in partial satisfaction of the

requirements for the degree of

Doctor of Philosophy

in

Engineering – Materials Science and Engineering

in the

Graduate Division

of the

University of California, Berkeley

Committee in charge:

Professor Robert O. Ritchie, Chair

Professor Kevin Healy

Professor Tony M. Keaveny

Spring 2010

The Effects of Obesity on Murine Cortical Bone

© 2010

by Sophi Martin

## **ABSTRACT**

The Effects of Obesity on Murine Cortical Bone

by

Sophi Martin

Doctor of Philosophy in Engineering – Materials Science and Engineering

University of California, Berkeley

Professor Robert O. Ritchie, Chair

This dissertation details the effects of obesity on the mechanical properties and structure of cortical bone. Obesity is associated with greater bone mineral content that might be expected to protect against fracture, which has been observed in adults. Paradoxically however, the incidence of bone fractures has been found to increase in overweight and obese children and adolescents. Femora from adolescent and adult mice fed a high-fat diet are investigated for changes in shape, tissue structure, as well as tissue-level and whole-bone mechanical properties. Results indicate increased bone size, reduced size-independent mechanical properties, but maintained size-dependent mechanical properties. Other changes in cortical bone response to obesity are observed with advancing age. This study indicates that bone quantity and bone quality play important compensatory roles in determining fracture risk, and that fracture risk may not be lessened for adults as previously thought.

## **DEDICATIONS**

This dissertation is dedicated to my loving husband Lane as well as my parents Irina and Stanislav. You each inspired me to be the best I could be and supported me along my path in innumerable ways, for which I thank you from the bottom of my heart.

## TABLE OF CONTENTS

LIST OF FIGURES .....	.v
LIST OF TABLES .....	.ix
LIST OF SYMBOLS & ABBREVIATIONS .....	.x
ACKNOWLEDGEMENTS .....	.xiv
CHAPTER 1 – Introduction to Obesity and Cortical Bone .....	1
1.1 – Prevalence of Obesity and the Relationship of Obesity to Fracture Risk .....	2
1.2 – Prior Work .....	3
1.3 – Factors in the Obesity – Fracture Risk Link .....	4
1.4 – Organization of this Dissertation and Summary of Findings Herein .....	6
CHAPTER 2 – General Methodologies .....	7
2.1 – Quantifying extent of obesity and hormonal effects .....	8
2.1.1 – <i>body weight, fat percentage, bone mineral content and areal density</i> .....	8
2.1.2 – <i>hormone evaluation</i> .....	9
2.1.3 – <i>non-enzymatic glycation</i> .....	9
2.1.4 – <i>bone histomorphometry measurements</i> .....	10
2.2 – Mechanical testing of cortical bone .....	10
2.2.1 – <i>Elastic behavior and strength measurement on femora</i> .....	10
2.2.2 – <i>Fracture toughness measurement on femora</i> .....	12
2.2.3 – <i>Structural evaluation of femora</i> .....	18
2.3 – Statistics .....	22
CHAPTER 3 – Effects of Obesity on Cortical Bone in Young Mice .....	24

3.1 – Childhood obesity and fracture risk . . . . .	25
3.2 – Results of High-Fat Diet-Induced Obesity on Young Mice . . . . .	25
3.2.1 – <i>Metabolic Phenotype of Experimental Animals: Validation of Obesity Model</i> . . . . .	25
3.2.2 – <i>Bone Densiometry Studies</i> . . . . .	26
3.2.3 – <i>Bone geometry changes as a result of high-fat diet</i> . . . . .	28
3.2.4 – <i>Mechanical testing: evaluation of tissue quality via size-independent mechanical measures and whole-bone behavior via size-dependent measures</i> . . . . .	28
3.2.5 – <i>Structural characterization: mineral organization and lamellar alignment of cortical bone</i> . . . . .	30
3.2.6 – <i>Correlation Analysis</i> . . . . .	32
3.3 – Discussion of Young Mouse Results . . . . .	34
CHAPTER 4 – Changes in Cortical Bone Response to High-Fat Diet from Adolescence to Adulthood in Mice . . . . .	36
4.1 – Fracture risk in adults versus adolescents . . . . .	37
4.2 – Results of High-Fat Diet-Induced Obesity on Young and Adult Mice . . . . .	38
4.2.1 – <i>Metabolic Phenotype of Experimental Animals: Validation of Obesity Model</i> . . . . .	38
4.2.2 – <i>Bone densitometry</i> . . . . .	38
4.2.3 – <i>Bone geometry</i> . . . . .	41
4.2.4 – <i>Bone histomorphometry measurements: cross-sectional geometry increases for both age groups while periosteal and endosteal response is different in young vs. adult</i> . . . . .	41
4.2.5 – <i>Non-enzymatic glycation shows increase of AGEs with obesity</i> . . . . .	43
4.2.6 – <i>Mechanical testing: Mechanical properties decrease with obesity</i> . . . . .	43
4.2.7 – <i>Structural characterization: mineral organization and lamellar alignment of cortical bone is reduced in obese mice</i> . . . . .	43
4.2.8 – <i>Correlation Analysis</i> . . . . .	45
4.3 – Discussion of Adult versus Young Mouse Results . . . . .	47
CHAPTER 5 – Summary and Future Work . . . . .	49

5.1 – Summary of findings .....	49
5.1.1 – Summary of Chapter 1.....	49
5.1.2 – Summary of Chapter 2.....	49
5.1.3 – Summary of Chapter 3.....	49
5.1.4 – Summary of Chapter 4.....	49
5.2 – Directions for Future Work .....	50
APPENDIX A – Diet formulation .....	51
A.1 – Control Chow for Young Study.....	51
A.2 – HFD for both studies, D12450B is the control diet for the young vs. adult study .....	52
APPENDIX B – Leptin ELISA kit.....	53
APPENDIX C – IGF-I ELISA kit .....	55
APPENDIX D – Blood glucose meter .....	56
APPENDIX E – Blood glucose results for young study (Chapter 3).....	58
REFERENCES .....	60



## LIST OF FIGURES

Figure 1.1 Prevalence of obesity among U.S. Adults. As of 2007, at least 15% of adults in every state are deemed obese (BMI $\geq$ 30.0). . . . .	2
Figure 1.2 Mesenchymal stem cells and adipocyte derived hormones. Adipocytes and osteocytes develop from mesenchymal stem cells. Adipocytes have the capability of releasing hormones, such as adiponectin, leptin, and estrogen which can affect osteocyte and osteoblast differentiation and proliferation. . . . .	5
Figure 2.2 Representative stress-strain curve. Yield stress is determined at the 0.2% strain offset, maximum stress is determined from the maximum point on the curve, and failure stress is the final stress the bone sees prior to complete failure. Bending modulus is given by the slope of the linear portion of the stress-strain curve. . . . .	12
Figure 2.3. Schematic diagram of mechanical testing setup and location of data collection. (a) Unnotched and notched specimens were loaded as pictured, with the ends of the bone cut off and the posterior section of the bone resting on the two support pins. (b) shows the location of the break in notched samples, and (c) shows a schematic of the measurement of the half-crack angles. To measure the half-crack angle for the <i>crack-initiation</i> and <i>maximum load</i> methods for calculating $K_c$ , the half-crack angle for the notch is defined in the left-hand figure. Two lines should be extended from the geometric center of the bone (located by the intersection of major and minor axes) to the edge of the notch. These lines should terminate in the middle of the cortical wall. For the <i>fracture instability</i> method, the same process should be applied, except the lines should terminate at the boundary of the stable crack-growth region and the unstable crack-growth region, as shown by the right-hand figure. . . . .	14
Figure 2.4. SEM image showing the machined notch, region of stable crack growth, and the region of unstable fracture, used to measure the crack size (half-crack angle) for the instability method of determining the fracture toughness. This micrograph is of a mouse femur; the inset shows the region of the cortex where the image was taken. . . . .	16
Figure 2.5. Representative load-displacement curve for a sharply-notched bend specimen. On the plot are the constructions for the determination of the loads $P_Q$ , $P_{max}$ , and $P_f$ used to compute the fracture toughness $K_c$ . $P_Q$ is given by the intersection of the loading curve with a line that has a 5% lower slope than the elastic deformation slope (5% secant construction), $P_{max}$ is given by the maximum load, and $P_f$ is given by the load at unstable fracture (instability). The loads are used with Eq. 12 to calculate the <i>crack-initiation</i> , <i>maximum load</i> , and <i>fracture instability</i> toughnesses, respectively. . . . .	17

Figure 2.6 Nanoindentation load-displacement curve. From W. C. Oliver & G. M. Pharr, J Mater Res 19, 3 (2004). . . . . 21

Figure 3.1. Validation of Obesity Model: Body Composition, Serum Leptin Concentration, and Bone Mineral Measures. (a) Representative HFD and Chow mice. Typical HFD mouse (top) and typical Chow mouse (bottom) at the conclusion of the 19 week diet period; (b) Average weekly weights of Chow and HFD groups. Horizontal axis is mouse age in weeks; (c) lean body mass (left) and fat body mass (right) for Chow and HFD groups at conclusion of study; (d) serum leptin concentration at conclusion of study; (e) serum IGF-I concentrations at the conclusion of study. No difference was observed in lean mass, but significant increase in the fat mass and in leptin concentration for the HFD group.  $n=15$  for the Chow group and  $n=14$  for HFD group. (\*  $P<0.01$ , \*\*\*  $P<0.001$ ) . . . . . 27

Figure 3.2. Bone quantity measures – Bone mineral (a) Whole-body bone mineral content (BMC); BMC is higher in the HFD group, which is expected because bones are larger (\*\*\*  $P<0.001$ ). (b) Whole-body areal bone mineral density (aBMD) is unchanged, which is not surprising as the lean body mass was unchanged (see Fig. 1). (c) Bone mineral content of the spine and (d) areal bone mineral density of the spine are significantly higher as a result of HFD (\*  $P<0.05$ ). (e) volumetric bone mineral density (vBMD) of the femoral cortical bone as well as (f) femoral BMC and (g) are not significantly different between groups. . . . . 29

Figure 3.3. Cortical bone quantity measures – Bone size: (a) Average cortical thickness; (b) outer cortical thickness; (c) inner cortical radius; (d) cortical cross-sectional area; and (e) second moment of area. Significant increase (\*  $P<0.05$ ; \*\*  $P<0.01$ ) for the HFD group is observed for all measures except (f) femoral length. (g) Whole-body bone mineral content (BMC); BMC is higher in the HFD group, which is expected because bones are larger (\*\*\*  $P<0.001$ ). (f) Whole-body areal bone mineral density (aBMD); and (i) volumetric bone mineral density (vBMD) of the femoral cortical bone are not significantly different between groups, which is not surprising as the lean body mass was unchanged (see Fig. 1).  $n=15$  for the Chow group and  $n=14$  for HFD group. . . . . 29

Figure 3.4. Cortical bone quality: whole-bone and tissue-level mechanical property measurements: (a) Yield strength; (b) maximum strength; (c) bending stiffness; (d) fracture toughness,  $K_c$ ; (e) yield load; (f) maximum load; (g) yield strain; and (h) maximum strain. Measured size-independent mechanical properties (except strain) were significantly decreased for HFD group vs. Chow group despite increased bone size (a-f); these parameters are an indication of bone-tissue quality. Size-dependent measures which address whole-bone behavior (specifically, load) did not differ between groups indicating a compensatory mechanism between bone size and tissue quality.  $n=15$  for the Chow group and  $n=14$  for HFD group (\*  $P<0.05$ ; \*\*  $P<0.01$ ; \*\*\*  $P<0.001$ ). . . . . 30

Figure 3.5. Through-wall SEM images of fracture region showing tissue structure at the whole-bone scale. (a) Cortical wall in bone from Chow group; (b) Cortical wall in HFD group. The scale bar indicates 100  $\mu$ m. The medial cortex in HFD bone (b) shows reduced alignment of osteocyte lacunae and reduction in lamellar alignment at the tissue level. These images are representative of five samples each of HFD and Chow. The inset indicates that images were taken from vertical sections through a region beyond the notch at the crack surface. The dark grey region indicates the notch, and the arrow indicates direction of crack growth, with crack propagation happening evenly from both sides of the notch. . . . . 31

Figure 3.6. High-magnification TEM images of structure and mineral organization. (a) Mineral organization of bone from Chow group; and (b) mineral organization of bone from HFD group. The scale bar indicates 200 nm. Mineral appears more poorly aligned and organized in HFD bone than in Chow bone, suggesting a reduction in microstructural tissue quality. . . . . 32

Figure 4.1. Validation of Obesity Model: Body Composition, Serum Leptin Concentration, IGF-I Concentration. (a) Average weekly weights of Chow and HFD groups. Horizontal axis is mouse age in weeks; (b) adult and (f) young lean body mass; adult (c) and (g) young fat body mass for Chow and HFD groups at conclusion of study; adult (d) and (h) young serum leptin concentration (reported in mean  $\pm$  st. err.) at conclusion of study; adult (e) and (i) young serum IGF-I concentrations at the conclusion of study. Both lean body mass and fat body mass increased, but significant increase in the fat mass and in leptin concentration for the HFD group. aChow  $n=13$ , aHFD  $n=14$ , yChow  $n=15$ , yHFD  $n=15$  (\*\*  $P<0.01$ , \*\*\*  $P<0.001$ ). . . . . 39

Figure 4.2. Bone mineral. Adult (a) and young (e) whole-body bone mineral density (aBMD) is unchanged in HFD; adult (b) and young (f) whole-body areal bone mineral content (BMC) is lower for the yHFD vs. yChow, which is likely due to reduced spinal aBMD. Adult (c) and young (g) areal bone mineral density of the femora are unchanged; Adult (d) and young (h) areal bone mineral density of the spine are reduced for HFD despite increasing weight, leptin, and IGF-I. aChow  $n=13$ , aHFD  $n=14$ , yChow  $n=15$ , yHFD  $n=15$  (\*\*  $P<0.001$ ). . . . . 40

Figure 4.3. Cortical bone size. Adult (a) and young (e) moment of area at the dyaphysis is unchanged in HFD; adult (b) and young (f) cortical thickness is reduced in adults. Adult (c) and young (g) femoral diameters are increased in yHFD vs. yChow; Adult (d) and young (h) femoral lengths are unchanged. The general trend, although not significant points to decreasing bone size in adults and increasing bone size in young obese mice compared to Chow. aChow  $n=13$ , aHFD  $n=14$ , yChow  $n=15$ , yHFD  $n=15$  (\*  $P<0.01$ ). . . . . 42

Figure 4.4. Cortical bone quality: whole-bone and tissue-level mechanical property measurements. Adult (a) and young (f) bending modulus; adult (b) and young (g) maximum load; adult (c) and young (h) yield stress; adult (d) and young (i) max stress; adult (e) and young (j) fracture toughness. Measured size-independent mechanical properties were significantly decreased for HFD group vs. Chow groups despite (modulus, yield and max stress, and fracture toughness); these parameters are an indication of bone-tissue quality. Size-dependent measures which address whole-bone behavior (specifically, load) also declined for HFD at both ages, likely due in part to modest bone size changes, as bone size was not able to compensate for poor mechanical quality. aChow  $n=13$ , aHFD  $n=14$ , yChow  $n=15$ , yHFD  $n=15$  (\*  $P<0.05$ ; \*\*  $P<0.01$ ).  
 ..... 44

Figure 4.5. SEM images of of fracture region showing tissue structure changes at the posterior region. (a) aChow group; (b) aHFD; (c) yChow; (d) yHFD. The scale bar indicates 20  $\mu\text{m}$ . The posterior cortex in HFD bone (b) and (d) shows reduced alignment of osteocyte lacunae and reduction in lamellar alignment at the tissue level. These images are representative of three samples each of aHFD, yHFD, aChow, and yChow. Medial, lateral, and anterior portions of the bone sections appeared similar for HFD and Chow in both age groups. .... 45

Figure A1. Blood glucose levels after 4 hour fasting in young study. (a) Blood glucose levels at age 15 weeks; (b) blood glucose levels at age 21 weeks; (c) baseline blood glucose levels in glucose tolerance test at age 22 weeks; (d) glucose tolerance test curve at age 22 weeks. At week 21, two HFD mice exhibited blood glucose levels over 200 mg/dL, and at week 22, 10 out of 15 HFD mice were hyperglycemic. One mouse at age 22 weeks had uncontrolled diabetes and died shortly prior to the conclusion of the study. ....59

## LIST OF TABLES

Table 1. Correlation coefficients between standardized properties in bone from (a), (c) Chow and (b), (d) HFD groups. Coefficients from correlation analysis applied between standardized mechanical properties and standardized bone and physiological properties of (a) Chow group and (b) HFD group. In cases where measurements were related and highly positively correlated, a composite score was used in the analysis. Bone size is the largest predictor of mechanical properties, more so than bone-mineral measures or body composition. Interestingly, size-independent measures of bone quality are most affected by the size of the bone, which implies a reduced quality with increasing quantity. Correlation coefficients between body mass measures and bone size measures show that LBM is positively correlated with bone size in both groups (c) & (d), and that FBM is very weakly negatively correlated with bone size. HFD (d) was almost significant for LBM-bone size correlation ( $P=0.053$ ). . . . . 33

Table 2. Correlation coefficients between standardized properties in bone from (a)-(d) adult and (e)-(h) young groups. Coefficients from correlation analysis applied between standardized mechanical properties and standardized bone and physiological properties of (a), (c) adult Chow group; (b), (d) adult HFD group; (e), (g) young Chow group; (f), (h) young HFD group. In cases where measurements were related and highly positively correlated, a composite score was used in the analysis. Bone size is the largest predictor of mechanical properties, more so than bone-mineral measures or body composition. Interestingly, size-independent measures of bone quality are most affected by the size of the bone, which implies a reduced quality with increasing quantity. Correlation coefficients between body mass measures and bone size measures show that LBM is positively correlated with bone size in both groups (c), (d), (g), (h) and that FBM is very weakly negatively correlated with bone size. . . . . 46

## LIST OF SYMBOLS & ABBREVIATIONS

$\alpha$  – fitting parameter for Ramberg-Osgood constitutive relationship

$\varepsilon$  – strain

$\varepsilon_o$  – reference strain for Ramberg-Osgood constitutive relationship

$\lambda$  – wavelength of incident radiation in the Bragg equation

$\nu$  – velocity of a sound wave, Poisson's ratio

$\mu$  – x-ray attenuation efficiency

$\Theta$  – half-crack angle

$\Theta_c$  – critical half-crack angle

$\Theta_{init}$  – half-crack angle at initiation

$\rho$  – density of material

$\sigma$  – stress

$\sigma_b$  – bending stress

$\sigma_o$  – reference stress for Ramberg-Osgood constitutive relationship

$\sigma_u$  – maximum stress

$\sigma_y$  – yield stress

$a_c$  – critical notch length

$a_{init}$  – initiation notch length

A – cortical cross-sectional area

aBMD – areal bone mineral density

aChow – adult group fed control diet in second study

AGEs – advanced glycation end-products

aHFD – adult group fed high-fat diet in second study

BDMA – benzlydimethylamine

BFR/BS – bone formation rate per unit bone surface

BMC – bone mineral content

BMD – bone mineral density

$c$  – distance from center of mass to periosteal surface

Ca – calcium

Chow – standard laboratory control diet

Ct. – cortical

$d$  – displacement

DXA – dual x-ray absorptiometry

$E$  – Young's modulus, bending modulus

EDTA – ethylenediaminetetraacetic acid

ELISA - enzyme-linked immunosorbent assay

$F$  – applied force

FA - fluoroapatite

FBM – fat body mass

HA – hydroxyapatite

HCl – hydrochloric acid

HFD – high-fat diet

$I$  – cross-sectional moment of inertia, incident energy in DXA

IGF-I - insulin-like growth factor I

$J$  – nonlinear-elastic fracture toughness

$J_{pl}$  – plastic portion of nonlinear-elastic fracture toughness

$K_c$  – critical value of linear-elastic fracture toughness

$K_I$  – mode-I linear-elastic fracture toughness

keV – kilo-electron volt

LBM – lean body mass

$m$  – mass

$M$  – bending moment

$M_o$  – reference bending moment Ramberg-Osgood constitutive relationship

MNA – methyl nadic anhydride

M.A. – second moment of area

MAR – mineral apposition rate

$MgF_2$  – magnesium fluoride

MS/BS – mineralizing surface per unit bone surface

$n$  – sample size

NEG – nonenzymatic glycation

NPY – neuropeptide Y

$P$  – significance

$P_c$  – critical load

$P_f$  – load at fracture

$P_Q$  – reference load

$P_u$  – maximum load

$P_y$  – yield load

qBEI – quantitative back-scattering electron imaging

$R_i$  – inner cortical radius



$R_m$  – mean cortical radius

$R_o$  – outer cortical radius

$S$  – full span of support pins in three-point bending

SE(B) – single-edge notched three-point bend specimen geometry

SEM – scanning electron microscopy

SR $\mu$ CT – X-ray micro-tomography

$t$  – cortical thickness

TEM – transmission electron microscopy

vBMD – volumetric bone mineral density

wt% - weight percent

yChow – young group fed control diet in second study

yHFD – young group fed high-fat diet in second study

$Z$  – atomic number

## ACKNOWLEDGEMENTS

This work was primarily supported by my advisor, Professor Robert O. Ritchie, who is funded by the Laboratory Directed Research and Development Program of Lawrence Berkeley National Laboratory (LBNL), funded by the U.S. Department of Energy under contract no. DE-AC02-05CH11231. Rob was a great source of advice, both technical and otherwise throughout this work and my graduate career. Without him, such a work of intense collaboration between institutions would not be possible. Joel Ager is also acknowledged as a great collaborator offering advice and insight, especially in general tenacity throughout graduate studies as well as more technical aspects such as statistics.

Animal study work was supported Tamara Alliston and Christian Vaisse, as well as their students and postdocs Carol Chen, Jen Wade, and Simon Tang, of University of California San Francisco, who are funded by the National Institutes of Health under grant nos. RO3DE016868 and RO1-60540, 68152, as well as American Heart Association CDA 740041N. Tamara and Christian were also instrumental in providing advice and insight about the studies. Such an interdisciplinary study could not be conducted without a great dedication of time from experts in such disparate fields.

Transmission electron microscopy work was supported by the British Council. I acknowledge Holly Barth for the x-ray synchrotron micro-tomography performed at beamline 8.3.2 at the Advanced Light Source at LBNL, supported by the Office of Science of the Department of Energy. The laboratory of Dr. Raffaella Carzaniga in the Electron Microscopy Centre at Imperial College London (South Kensington campus) is also acknowledged where TEM sample preparations were performed. I acknowledge the laboratories of Ramamoorthy Ramesh at UC Berkeley and Scott Robinson at Beckman Institute (UI Urbana-Champaign, IL) where SEM work was performed. I also acknowledge Drs. Wei Yao and Mohammed Shahnazari and Prof. Nancy Lane from UC Davis Department of Internal Medicine for the calcien labeling experiments and interpretation of data.

Finally, I acknowledge my thesis committee, Prof. Tony Keaveny and Prof. Kevin Healy, for dedicating the time to help me perfect my thesis and offer guidance in my last phase of graduate school.

## **Chapter 1 – Introduction to Obesity and Cortical Bone**

This chapter gives an introduction to the prevalence of obesity in the United States and bone fracture risk patterns in relation to obesity trends. Additionally, biological interactions of fat and bone are reviewed along with prior work in the field of fracture risk and obesity. The central focus of this work is to understand how obesity is linked to cortical bone mechanical properties, and in this light, a possible route of investigation is presented. Finally, the chapter concludes with a summary of the organization of this dissertation and summary of the findings herein.

## Chapter 1.1 – Prevalence of Obesity and the Relationship of Obesity to Fracture Risk

Obesity is an increasingly prevalent medical condition,<sup>1</sup> which is often associated with other medical problems such as diabetes and heart disease.<sup>2</sup> According to a study done by the American Medical Association, the prevalence of obesity in the United States (body mass index, or BMI  $\geq 30.0$ ) increased from 22.9% in 1994 to 30.5% in 2000.<sup>1</sup> Additionally, the prevalence of overweight individuals, i.e., any individual with BMI  $\geq 25.0$ , increased from 55.9% to 64.5% in the same time period and extreme obesity (BMI  $\geq 40.0$ ) increased from 2.9% to 4.7%. Figure 1.1 shows the prevalence of adult obesity per state.<sup>3</sup> The American Medical Association also found that 31% of children aged 6 through 19 were at risk of developing obesity (95<sup>th</sup>  $\geq$  BMI  $\geq$  85<sup>th</sup> percentile for sex/age/height) and that an additional 16% were obese (BMI  $\geq$  95<sup>th</sup> percentile for sex/age/height).<sup>4</sup> Obesity has been associated with increased risks of diabetes, cholelithiasis, hypertension, coronary heart disease, and some cancers.<sup>2</sup> As the prevalence of overweight and obesity increases, related medical complications and medical treatment costs are sure to rise.

Increasing weight has also been linked to changing bone fracture prevalence and some studies suggest that it can be protective against osteoporosis and related fractures. A number of public health studies have linked obesity, especially in older adults, with increased bone-mineral density (BMD) and content (BMC).<sup>5,6,7,8,9,10,11,12</sup> Increases in BMD and BMC have been associated clinically with a reduction of fracture incidence<sup>6,13</sup> and, therefore, an increase in BMD/C as is often observed in obesity is associated with a reduced risk of fracture. Additionally, lower rates of fracture have been reported in obese

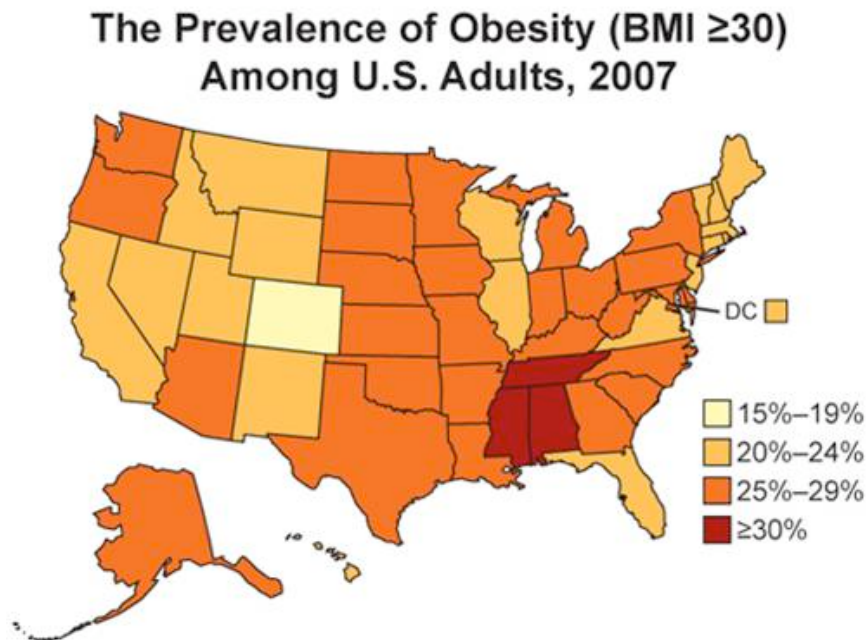


**Figure 1.1 Prevalence of obesity among U.S. Adults.** As of 2007, at least 15% of adults in every state are deemed obese (BMI  $\geq 30.0$ ).<sup>3</sup>

adults.<sup>14</sup> Conversely, an increased fracture incidence has been observed in adolescents and children who are overweight or obese.<sup>15</sup> Taylor *et al.*, find that the rate of skeletal misalignment and joint discomfort is increased in overweight and obese children,<sup>15</sup> decreasing the likelihood that overweight children will participate in an active lifestyle, thereby increasing health risks later in life. Children and adolescents who are overweight tend to also have poorer posture control and body position sense than their normal weight peers<sup>16,17,18</sup>, which is likely a contributing factor in the observed increase in fractures.

In this context, the question arises whether obesity can be related in a scientifically sound manner to microstructural and mechanical behavior changes in bone (*i.e.*, to *bone quality*) in addition to higher bone mass (*bone quantity*) and if this can explain the previously observed changes in fracture risk in relation to increasing weight. The goal of this work to explore how mechanical properties as well as geometric parameters of cortical bone change in response to an obesity-inducing diet. It is the aim of this study to evolve beyond the passive observation reported in the public health studies to apply traditional mechanical testing and rigorous fracture mechanics to biomaterials such as cortical bone.

## Chapter 1.2 – Prior Work

Obesity is a much-studied topic among the public health community. One point of interest is the effect of obesity on bone fracture risk, and accordingly, some studies have attempted to quantify the relationship between obesity and fracture incidence. Although no direct evaluation of cortical mechanical properties is possible in a longitudinal study investigating the effects of weight gain, there have been reports of increased geometrical parameters such as cortical thickness, as well as increased bone mineral density and content in people who are overweight and obese compared to underweight and normal weight individuals.<sup>12,19,20,21,22</sup> In turn, these studies suggest that obesity is protective against osteoporosis, a disease defined by low BMD scores, as well as fracture in general. Clinical bone mineral measures are two-dimensional, and are therefore indicative not only of volumetric bone density, but also of bone size. Since a typical BMD measurement divides a measured BMC (from x-ray attenuation) by the *area* of bone scanned, reported BMD measures in many of these public health studies are confounded by changes in bone size parameters such as cortical thickness or even height.<sup>23</sup>

Due to the limitations of public health studies in evaluating the tissue-level effects of obesity in a systematic manner, animal studies are required. Surprisingly, only a few studies have addressed the question of bone quality and quantity in response to obesity using animal models. Rat studies have found reductions in yield and maximum stresses, energy absorption, structural rigidity and failure loads, despite larger bone sizes as a result of high-fat and high-sugar diet-induced obesity.<sup>24,25,26</sup> Brahmabhatt *et al.*,<sup>24</sup> find that a month of high-fat diet in male adult rats produces increases in femoral cortical thickness and cross-sectional area and an increase in energy absorption capacity (defined as an area under a load-displacement curve). Li *et al.*,<sup>25</sup> find that ten weeks of high-fat, high-sucrose diet in adult rats increases the cross-sectional area of the metatarsal and decreases the maximum load and energy at failure in the tibia. Finally, Zernicke *et al.*,<sup>26</sup> conducted a long-term study (2 years) on the effects of high-fat, high-sucrose diet on rats

and found lower energy at proportional limit and at maximum as well as total energy absorbed in the femoral neck. They also found reduced cortical shell proportion to total area in the femoral neck. The conclusions of these various studies are not completely consistent; however, in general, a significant *decrease* in mechanical performance (reduced bone quality) concurrent with an *increase* in bone size (increased bone quantity) has been reported.

These prior animal studies have focused primarily on properties such as failure load and energy absorption, which do not account for changes in the bone cross-section area, thereby confounding the effects of bone quality and quantity. To fully understand the mechanical integrity of the bone and its resistance to fracture, *size-independent* mechanical properties should be measured,<sup>27</sup> including yield and maximum stresses, stiffness and fracture toughness. Strength, defined by the yield stress at the onset of permanent deformation or maximum strength at the peak load before fracture, is a measure of the force/unit area that the bone can withstand. Stiffness is related to the elastic modulus and defines the force required to give a specific elastic strain. The fracture toughness measures resistance to fracture. Additionally, although most prior studies have involved rats, the use of mice allows for greater genetic control which could be used in future studies to identify specific biological factors that are responsible for the high-fat diet-induced changes in bone.

### **Chapter 1.3 – Factors in the Connection between Obesity and Fracture Risk**

Many biological systems are affected by obesity; both the physical weight and the fat tissue itself can influence the function of organs and metabolic systems. The first interesting link between fat and bone appears in the origin of the cells making up these structures. Adipose cells and osteocytes are both derived from the same mesenchymal stem cells. Once fully developed, adipocytes can secrete a variety of hormones which can affect bone both locally and through the sympathetic nervous system. As a result, the response of bones to obesity is modulated through fat cells themselves, albeit indirectly.

Two possible ways by which obesity could affect bone properties are increased body mass and altered secretion of biological factors. Although the contribution of body mass to bone size and quality has been debated, it is well established that bone responds to external loads and that lean mass is more important than fat mass at predicting bone size and mineral density/content measures.<sup>28,29,30,31,32,33,34</sup> The latter observation is further supported by research showing that remodeling is influenced by dynamic rather than static loads.<sup>35,36</sup>

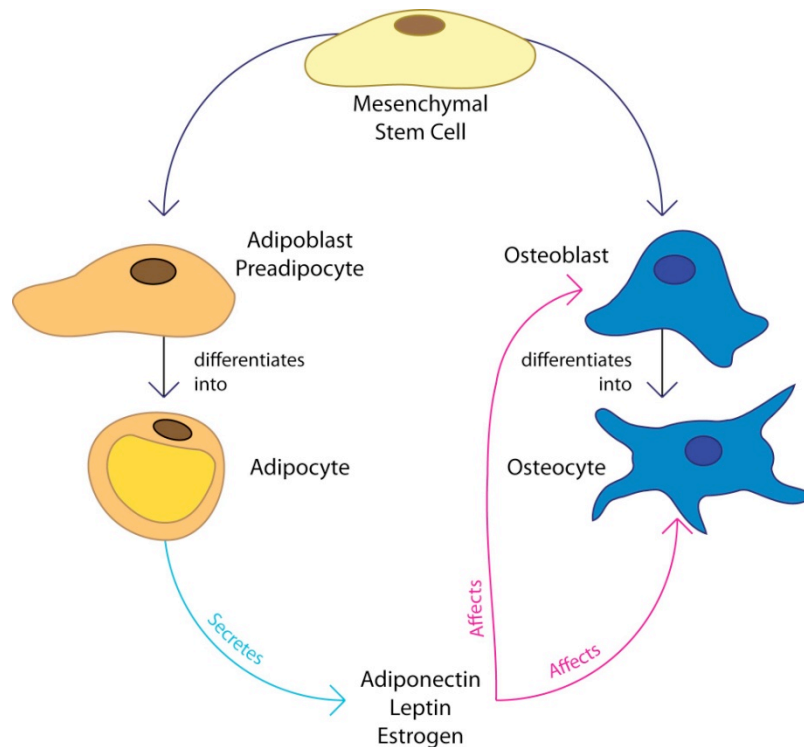


**Figure 1.2 Mesenchymal stem cells and adipocyte derived hormones.** Adipocytes and osteocytes develop from mesenchymal stem cells. Adipocytes have the capability of releasing hormones, such as adiponectin, leptin, and estrogen which can affect osteocyte and osteoblast differentiation and proliferation.

The levels of several hormones are altered by obesity, many of which can impact bone. Adipocyte-derived hormones such as leptin, adiponectin, and resistin also play a role in bone's response to obesity by a variety of mechanisms.<sup>9</sup> As leptin influences osteoblast activity both directly and indirectly through the central nervous system, it is typically considered in studies involving obesity and bone. Additionally, insulin-like growth factor I (IGF-I) has been observed to be reduced in caloric deprivation (and by extension, increased with increasing weight).<sup>37</sup> It has been suggested that IGF-I acts to increase bone size.<sup>38</sup> Therefore, as both increasing weight and changing bone size are expected in these studies, serum IGF-I and leptin levels were measured as part of the experimental method.

Despite the complex relationship between fat and bone, described succinctly in Ref. 9, it is evident that both fat mass and lean mass affect bone health. The purpose of this study is to determine whether diet-induced obesity affects bone-tissue quantity (bone size and mineral quantity measures), bone quality (defined by mechanical properties that affect fracture but are independent of bone size), or combinations of the two.

## **Chapter 1.4 – Organization of this Dissertation and Summary of Findings Herein**

The remainder of this text will be organized as follows: Chapter 2 will discuss all methods employed in the investigation of the effects of obesity on fracture risk, Chapter 3 will discuss the results of the first study looking into effects in young mice, Chapter 4 will discuss the results of the second study investigating differences in effects in young versus adult mice, and Chapter 5 will summarize the work and postulate on further directions for research. In young mice, the effects of obesity on bone fracture are such that bone quantity (i.e. bone size and mineral content) balance with bone quality (i.e. mechanical performance and structural integrity) to maintain bone performance (i.e. load to failure). In the second study, however, we find that changes in body metrics (lean body mass specifically) occur where they did not in the first study. Also, cortical response shifts from periosteal in young to endocortical in adult and bone size changes shift from increasing bone size in young to decreasing bone size in adult. In general, there is a reduction in mechanical properties for both age groups, implying increased fracture risk for both age groups. Overall, these two studies indicate that although reduced fracture incidence is seen in obese individuals, cortical bone, in particular, is not to be regarded as being healthier than that of normal weight individuals.



## **Chapter 2 – General Methodologies**

This chapter gives an overview of the methodologies employed to investigate the effects of obesity on cortical bone in a murine model. First discussed are the methods employed to characterize the animal size and extent of obesity as well as pertinent hormonal levels which may impact the results observed in mechanical testing of femora. Following this discussion, methods for mechanical testing (three-point bend tests on femora, nanoindentation on cross-sections of femora), structural characterization (SEM, TEM, qBEI, and three-dimensional tomography, non-enzymatic glycation, calcein labeling, and finally statistical methods employed to evaluate for changes between groups are discussed in detail.

## Chapter 2.1 – Quantifying extent of obesity and hormonal effects

### Chapter 2.1.1 – Body weight, fat percentage, bone mineral content and areal density

The natural first step to take in any obesity study is to ensure that obesity is achieved successfully. In the studies discussed in this thesis, mice were housed five animals per cage and fed either a standard laboratory chow or a high-fat diet. In the case of the first study, the diet duration was 19 weeks, whereas the second study lasted 16 weeks. It is important to choose diets that have similar nutritional content (i.e. the high-fat and control diets are “matched”) to ensure that changes observed as a result of the diet do not stem from differing protein levels or other unknown confounding vitamin or mineral. The first study, which looks at obesity in young mice, did not use a matched diet, but the control diet (PicoLab Mouse Diet 21.6 kcal% fat, 55.2 kcal% carbohydrate, 23.2 kcal% protein) did have similar protein levels to the high-fat diet (Research Diets High-Fat Diet 60 kcal% fat, 20 kcal% carbohydrate, 20 kcal% protein). The follow-up study repeated the first experiment (30 young mice) and added an older study group (28 adult mice) to investigate effects of obesity in adults as compared to young/adolescents. Unlike the first study, the diet in the second study did contain a matched control for the high-fat diet. The diet information is given in complete detail in Appendix A.

To confirm whether the diet plan was successful, weekly weighing was conducted in the first study and bi-weekly weighing in the second. This confirmed that the high-fat diet mice were gaining weight faster than the chow mice and allowed for any weight-gain stabilization to be observable. The state of obesity was not specifically defined for the mice, but a significant proportion of body weight belonging to fat (i.e. >40%) as well as significant increases in weight compared to the chow group were clear indications that the mice on the high-fat diet were unhealthily overweight.

The fat proportions as well as lean body mass, fat body mass, and important bone mineral measures, such as whole-body bone mineral content and density, were determined using dual x-ray absorptiometry (DXA). This technique involves placing an anesthetized animal onto a platform below an x-ray source. The platform functions as an x-ray detector, and the DXA apparatus will measure the attenuation of x-rays at two distinct energies:

$$I = I_o \exp (-\mu_a m_a - \mu_b m_b) \quad (1)$$

$$I' = I_o' \exp (-\mu_a m_a - \mu_b m_b) \quad (2)$$

where  $I$  and  $I'$  are the two incident energies,  $m_a$  and  $m_b$  are the masses of two objects (i.e. fat and bone) which attenuate x-rays at different efficiencies, which are characterized by  $\mu_a$  and  $\mu_b$ .  $\mu_a$  and  $\mu_b$  are known from standardized experiments with control samples and solving equations (1) and (2) for two unknowns ( $m_a$  and  $m_b$ ) gives the masses of the components of interest (i.e. mass of fat and bone in an animal). Dividing this mass by the projected area of that tissue gives an areal bone mineral density (aBMD) in units of  $\text{g}/\text{cm}^2$ . This is a common technique to determine BMD in humans as well as animals, although it fails to capture the thickness dimension and therefore can underestimate the true volumetric bone mineral density. Further details of the technique and the concepts behind DXA can be found in a publication by Peppler and Mazess.<sup>39</sup>

### ***Chapter 2.1.2 – Hormone evaluation***

As already discussed, hormones play an important role in fat and bone and sometimes control their interactions with each other. Leptin, for example, impacts appetite control, bone turnover, and reproduction,<sup>40</sup> so its role in a fracture risk and obesity study is evident. Higher serum leptin concentrations are associated with increased weight in animals as well as higher bone mineral density and bone size.<sup>9</sup> In this study, serum leptin concentrations were measured via an enzyme-linked immunosorbent assay (ELISA) kit. Details for the specific kit used can be found in Appendix B. Additionally, insulin-like growth factor I (IGF-I) has been observed to be reduced in caloric deprivation (and by extension, increased with increasing weight).<sup>37</sup> It has been suggested that IGF-I acts to increase bone size.<sup>38</sup> Therefore, as both increasing weight and changing bone size are expected in these studies, serum IGF-I levels were measured via an Immunodiagnostic Systems Inc. Mouse/Rat IGF-I ELISA kit. Further details of this test are provided in Appendix C. Finally, it was important to determine whether any mice developed diabetes as diabetic animals have been shown to have altered fracture risks when compared to controls.<sup>41,42</sup> To address this question, blood-glucose levels were measured and a glucose tolerance test was performed after 4 hours of fasting (first study) and after an overnight fast (second study), using an Ascensia ELITE XL Blood Glucose Meter. Further details of this test are provided in Appendix D.

### ***Chapter 2.1.3 – Non-enzymatic glycation***

Non-enzymatic glycation (NEG) is a process by which sugars bind to amino residues in proteins to form molecular crosslinks in collagen known as advanced glycation end-products (AGEs). The formation of AGEs by NEG occurs spontaneously, and the accumulation of AGEs occur naturally with age as a consequence of poorer sugar metabolism and inefficient bone turnover. In general, higher concentrations are contraindicated for fracture resistance, and increased AGEs have been shown to reduce fracture toughness.<sup>43,44,45</sup> Higher AGEs would also be a logical consequence of a high-fat diet, which should increase blood glucose levels, to subsequently increase the rate of NEG. For these reasons, NEG has also been considered as part of the second study (adults vs. adolescents). In order to evaluate the extent of advanced glycation end-products (AGEs) in HFD and Chow bone, non-enzymatic glycation (NEG) was performed. The whole tibiae from the mice were demineralized using EDTA, and demineralization was confirmed using contact radiographs. The demineralized bone samples were then hydrolyzed using 6N HCl (24 hours, 110°C). AGEs content was determined using fluorescence readings taken using a microplate reader at the excitation wavelength of 370nm and emission wavelength of 440 nm and standardized to a quinine sulfate standard and normalized to the amount of collagen present in each sample. The amount of collagen for each bone sample was determined based on the amount of hydroxyproline. Hydroxyproline content was determined using a chloramine-T

colorimetric assay that recorded the absorbance of the digested samples against a hydroxyproline standard at the wavelength of 585nm.<sup>46</sup>

### ***Chapter 2.1.4 – Bone histomorphometry measurements***

To evaluate what portion of bone is growing at a specified time interval (usually several days before the end of a study), bone histomorphometry measurements are typically conducted as part of bone investigations. In the second study, where effects of obesity are considered in adult vs. adolescent mice, dynamic bone histomorphometric measures were obtained from midshaft tibia of each animal. Mice were injected with 10 mg/kg calcein 6 and 1 day before killing. At termination, tibiae were removed and fixed in 10% neutral phosphate-buffered formaldehyde for 24 h. Tibial mid-diphyseal regions were cut out using a precision saw (Isomet 1000, Buehler) and dehydrated in increasing concentrations of ethanol and embedded undecalcified in methylmethacrylate. Transverse sections (40  $\mu\text{m}$ -thick) of tibial cortex were cut at tibia-fibula junction using a diamond wire saw (Well 3241, Norcross, GA). The sections were coverslipped with Eukitt (Calibrated Instruments, Hawthorne, NY) and mounted unstained for visualization under fluorescent microscopy (Nikon, Eclipse E400, Japan) and quantitative morphometry using image analysis software (Bioquant Image Analysis Corporation, Nashville, TN). Endocortical and periosteal measurements included single- and double-labeled perimeter and interlabel width, which were used to calculate the mineralizing surface (MS/BS), mineral apposition rate (MAR), and bone formation rate (BFR/BS) according to the standard guidelines previously published.<sup>47</sup>

## **Chapter 2.2 – Mechanical testing of cortical bone**

### ***Chapter 2.2.1 – Elastic behavior and strength measurement on femora***

The elastic behavior of a solid can be measured in a variety of ways. A typical measure of interest is the elastic modulus, or Young's modulus  $E$ , which obeys the following relationship in isotropic materials:

$$E = \sigma/\varepsilon \quad (3)$$

where  $\sigma$  and  $\varepsilon$  are stress and strain, respectively, and  $E$  is the slope of the linear portion of the stress-strain curve under monotonic tension. The most accurate way to measure  $E$  is with an ultrasonic test which measures the velocity of sound through a solid piece of material. In this case, the velocity of a sound wave through the material is given by:

$$v = \sqrt{E/\rho} \quad (4)$$

where  $v$  is the velocity and  $\rho$  is the density of the material. The benefit of such an approach is that it yields the true modulus of the material, and additionally, it is non-destructive and repeatable on the same sample. The downside is that a regularly-shaped sample is needed to avoid complications due to sound waves bouncing off oddly angled surfaces. This complication can also arise for internal walls such as those belonging to

pores or holes. For these reasons, ultrasonic testing of mouse bones is not feasible and other options must be explored. Other options for testing methodology are tensile testing, microtesting, torsion, and bend. Tensile testing needs a precise specimen shape but can be very accurate if done in a careful manner. Microtesting, which involves machining small regularly shaped samples from whole bones, poses a danger for size-dependent effects as the method is susceptible to local structural heterogeneities. As bone is a complex structure, microtesting may miss important properties that exist above the structural size-scale investigated. Torsion is an easy test to perform but it is inaccurate for non-circular shapes. The test method remaining is bending.

Since femora are large enough to handle easily, are long and have a simpler cross-sectional geometry than other bones, they lend themselves easily to a bend test which can evaluate not only elastic behavior but also strength information.<sup>27</sup> This test is good for whole bones of small animals where precise machining is difficult. The ideal span-to-width ratio is 16:1 to minimize shear stresses which arise as a result of non-uniform bend moments present in a three-point bend configuration. One way to avoid this problem is to perform a four-point bend; however, a four-point bend test must exhibit equal loading on each loading pin for accurate results, and any irregularity in cross-sectional shape makes this requirement non-trivial. The downsides of the three-point bend test are that measured strains are only accurate pre-yield and that shear strains can account for up to 10-15% of measured deformation and therefore  $E$  is usually underestimated. Despite these shortcomings, the three-point bend test has the overwhelming benefit of being reproducible and very precise. While the true  $E$  may not be measured, the relative Young's moduli of a variety of treatment groups can be compared quite easily. An additional benefit of a bend test on femora is that it replicates a feasible biological load and may give some indication as to the relative behavior of femora under extreme stresses.

The methodology followed to determine stresses, strains, and bend modulus in bone follow the biomechanical testing procedures reviewed by Turner and Burr.<sup>27</sup> Due to the underestimation of Young's modulus in any whole-bone mechanical test, specifically a bend test in this scenario, the slope of the stress-strain curve which describes the elastic response in a three-point bend configuration will be called a "bend modulus" or  $E'$ . The following standard formulae show the relationships used to calculate stress, strain, and bend modulus from the load-displacement data (in load-control) of a three-point bend test<sup>27</sup>:

$$\sigma = FSc / 4I \quad (5)$$

$$\varepsilon = 12cd / S^2 \quad (6)$$

$$E' = FS^3 / 48dI \quad (7)$$

where  $F$  is the applied force,  $S$  is the full span of the lower support pins,  $c$  is the distance from the center of mass to the periosteal surface of the bone,  $I$  is the cross-sectional moment of inertia taken about the medial-lateral axis, and  $d$  is the measured displacement.

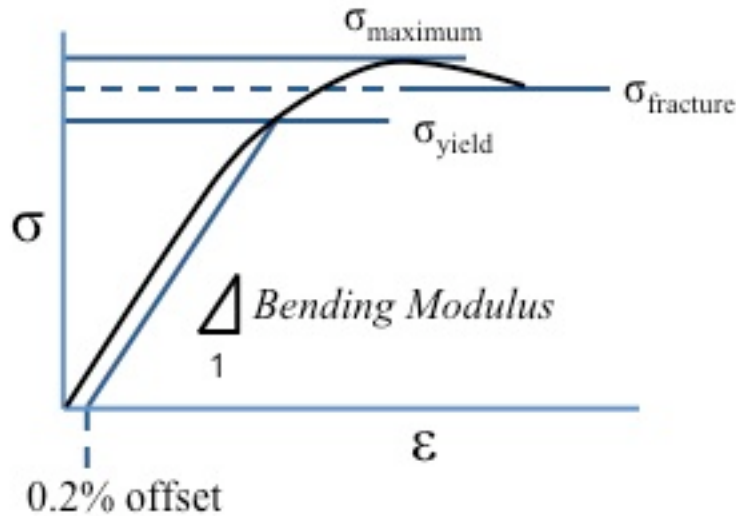


**Figure 2.2 Representative stress-strain curve.** Yield stress is determined at the 0.2% strain offset, maximum stress is determined from the maximum point on the curve, and failure stress is the final stress the bone sees prior to complete failure. Bending modulus is given by the slope of the linear portion of the stress-strain curve.

The yield stress, or where deformation is no longer elastic but has become irreversible, or plastic, is determined by a 0.2% strain offset, which is given by the intersection of a line parallel to the linear portion of the stress-strain curve drawn 0.002 strain away from the origin with the stress-strain curve. The maximum stress corresponds to the maximum point on the stress-strain curve and is analogous to an ultimate stress. See figures 2.2 and 2.3a for representative stress-strain curve and test set-up of a three-point bend test, respectively.

### ***Chapter 2.2.2 – Fracture toughness measurement on femora***

Femurs are the ideal mouse bones to evaluate the fracture toughness properties in small animal model studies. These bones are ~15 mm long with a ~1-2 mm diameter in mice, and can be readily tested in three-point bending. The ends of the bones are best cut-off with a low-speed saw, then notched and loaded such that the posterior surface is in tension and the anterior surface is in compression (Fig. 2.3). A notch can be created in the mid-diaphysis by “polishing” with a razor blade irrigated with 1  $\mu\text{m}$  diamond suspension; this razor micronotching technique<sup>48</sup> results in a consistently sharp notch with a root radius of ~10  $\mu\text{m}$ . All measurements need to be performed in fluid that simulates *in vivo* conditions, *e.g.*, Hanks’ Balanced Salt Solution (HBSS), at 37°C.

Since mouse bones are somewhat small to generate full R-curve behavior, particularly since this would involve the very difficult task of monitoring crack extension over such small dimensions, the best alternative measure of toughness is to determine a single-

valued  $K_c$ . As noted above, this involves testing the samples in three-point bending and measuring the load and crack length at crack initiation, maximum load or fracture instability. To calculate the mode I stress-intensity factor, solutions for circumferential through-wall cracks in cylindrical pipes,<sup>49,50</sup> can be used, where the value of  $K_I$  is given in terms of the wall (bone cortex) thickness  $t$ , mean radius  $R_m$  of the bone (to middle of the cortex), and crack length, defined in terms of the half-crack angle  $\Theta$  in Fig. 2.3c.

$$K_I = F_b \sigma_b \sqrt{\pi R_m \Theta}, \quad (8)$$

where  $F_b$  is a geometry factor,  $R_m$  refers to the mean radius, and  $\sigma_b$ , the applied bending stress, is calculated from the bending moment  $M$  ( $= PS/4$ ) in terms of the distance from the neutral axis,  $c$ , and area moment of inertia  $I$ , as  $\sigma_b = Mc/I$ . This solution is valid for both thin-walled and thick-walled bones, specifically for  $1.5 < R_m/t < 80.5$ , and for a range of half-crack angles,  $0 < \Theta/\pi < 0.611$ . Takahashi<sup>50</sup> assumed a thin-walled pipe solution to compute  $\sigma_b$ , namely:

$$\sigma_b = \frac{M}{2\pi R_m^2 t} \quad (9)$$

The moment of inertia about the axis of bending should, ideally, be computed with image analysis software. In terms of this moment of inertia about the medial-lateral axis, or  $I_{ML}$ , and the outer radius  $R_o$  the definition of  $\sigma_b$  is given by

$$\sigma_b = \frac{MR_o}{I_{ML}} \quad (10)$$

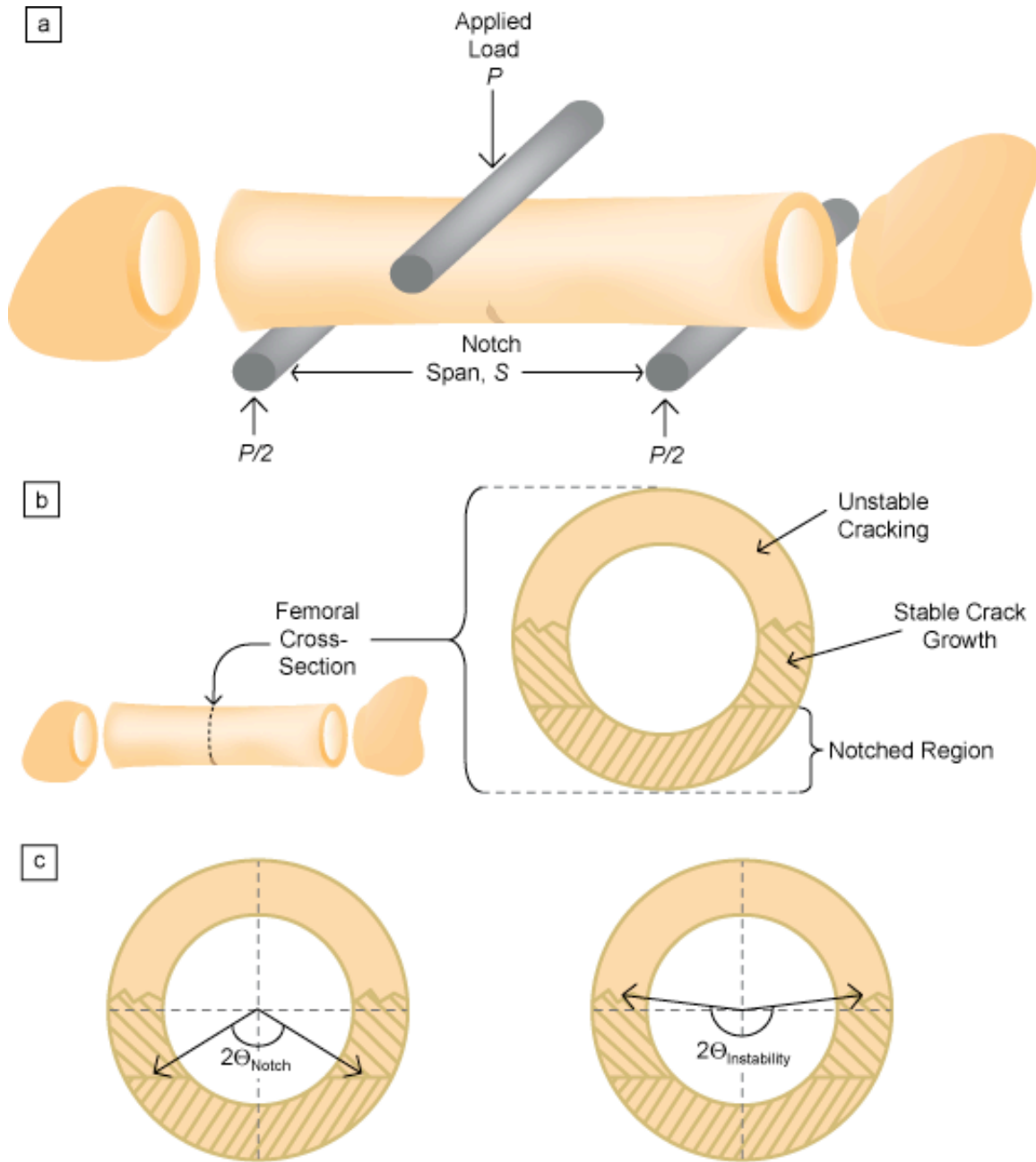


**Figure 2.3.** Schematic diagram of mechanical testing setup and location of data collection. (a) Unnotched and notched specimens were loaded as pictured, with the ends of the bone cut off and the posterior section of the bone resting on the two support pins. (b) shows the location of the break in notched samples, and (c) shows a schematic of the measurement of the half-crack angles. To measure the half-crack angle for the *crack-initiation* and *maximum load* methods for calculating  $K_c$ , the half-crack angle for the notch is defined in the left-hand figure. Two lines should be extended from the geometric center of the bone (located by the intersection of major and minor axes) to the edge of the notch. These lines should terminate in the middle of the cortical wall. For the *fracture instability* method, the same process should be applied, except the lines should terminate at the boundary of the stable crack-growth region and the unstable crack-growth region, as shown by the right-hand figure. Images (a) and (b) are reproduced from Ref. 51, and (c) is reproduced from Ref. 52.



Under these conditions,  $F_b$  is given by:

$$F_b = \left(1 + \frac{t}{2R_m}\right) \left[ A_b + B_b \left(\frac{\Theta}{\pi}\right) + C_b \left(\frac{\Theta}{\pi}\right)^2 + D_b \left(\frac{\Theta}{\pi}\right)^3 + E_b \left(\frac{\Theta}{\pi}\right)^4 \right] \quad (11)$$

where

$$A_b = 0.65133 - 0.5774\xi - 0.3427\xi^2 - 0.0681\xi^3$$

$$B_b = 1.879 + 4.795\xi + 2.343\xi^2 - 0.6197\xi^3$$

$$C_b = -9.779 - 38.14\xi - 6.611\xi^2 + 3.972\xi^3$$

$$D_b = 34.56 + 129.9\xi + 50.55\xi^2 + 3.374\xi^3$$

$$E_b = -30.82 - 147.6\xi - 78.38\xi^2 - 15.54\xi^3$$

$$\xi = \log\left(\frac{t}{R_m}\right)$$

These solutions assume a circular cross-section whereas long bones generally are far less uniform. A “propagation of errors” calculation through these “thick-walled pipe” stress-intensity solutions<sup>52</sup> shows that deviations of the bone dimensions away from a circular cross section with a uniform thickness have the greatest effect on the accuracy of the  $K$ -solution. An analysis of the resulting worst-case errors in computed stress-intensity values reveals an uncertainty of ~17%.

With respect to the point on the load-displacement curve where the toughness is measured, there are several approaches that can be employed to define the critical load  $P_c$  and crack size (*i.e.*, the half-crack angle  $\Theta$ ) used to compute the value of  $K_c$  (Fig. 2.3). For an intrinsic, crack-initiation toughness value, ideally the onset of cracking should be monitored independently and the load at crack initiation noted (*crack-initiation* method). As per the ASTM Standards,<sup>53</sup> this can be estimated by noting the load  $P_Q$  at the intercept of the load/displacement curve with a 5% secant line, *i.e.*, a line drawn from the origin with a slope 95% of the initial elastic loading line (this is intended to represent a crack extension of roughly 2% of the remaining ligament). However, for this latter (5% secant) construction to work, there must be limited plasticity (as this also affects the compliance slope); to ensure that this is the case, the E-399 Standard<sup>53</sup> also requires that  $P_u/P_Q \leq 1.1$  (where  $P_u$  is the maximum load) for a valid  $K_c$  result.

Due to the presence of plasticity in samples which are physically small, the 5% secant construction can be inaccurate in small animal studies. Accordingly, a more straightforward and simple way is to define instability at maximum load,  $P_c = P_u$ , and to use the length of the starter notch,  $a_c = a_{init}$  ( $\Theta_c = \Theta_{init}$ ) as the initial crack size (*maximum*

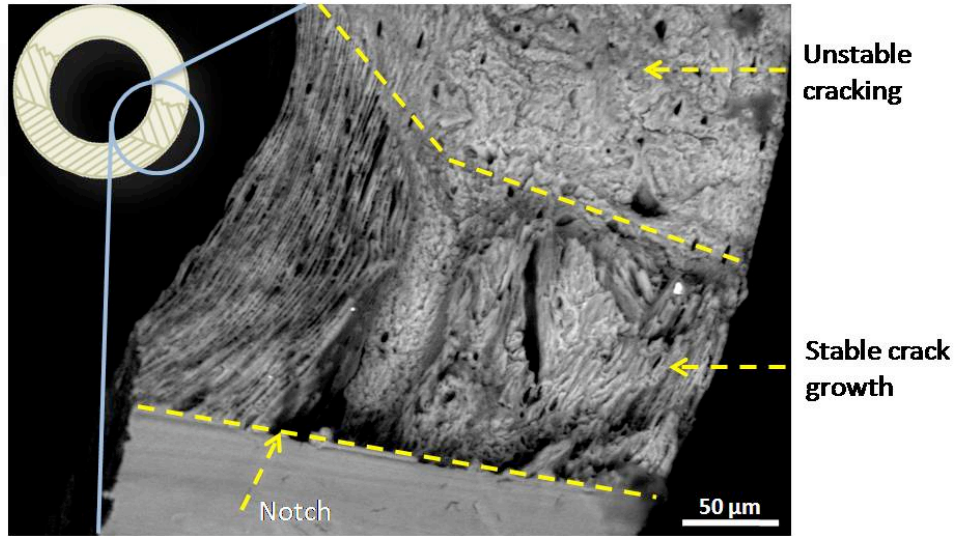


**Figure 2.4.** SEM image showing the machined notch, region of stable crack growth, and the region of unstable fracture, used to measure the crack size (half-crack angle) for the instability method of determining the fracture toughness. This micrograph is of a mouse femur; the inset shows the region of the cortex where the image was taken. Reproduced from Ref. 52.

load method). However, the latter approach is also liable to be inaccurate due to the possibility that some degree of subcritical (stable) cracking occurs prior to instability; moreover, in actuality, crack initiation rarely takes place exactly at maximum load. Since subcritical crack growth does occur in mouse femurs, an alternative, more accurate, approach is to take the load at fracture instability,  $P_f$ , and to use backscattered scanning electron microscopy (SEM) to determine the extent of subcritical cracking<sup>i</sup> in order to determine the corresponding crack size at instability  $\Theta_c = \Theta_{inst}$  (fracture instability method). Figure 2.4 shows an SEM image of the notch, region of stable crack growth, and the onset of overload fracture.

The “positions” of these various measurement points are shown schematically in Figure 2.5 which illustrates a load-displacement curve for a notched femur. In all three cases, the fracture toughness can be calculated from:

$$K_c = F_b \frac{P_c S R_o}{\pi(R_o^4 - R_i^4)} \sqrt{(\pi\Theta_c)}, \quad (12)$$

<sup>i</sup> Using SEM in the backscattering mode, subcritical cracking prior to instability can generally be detected by its different morphology from the machined starter notch and the final overload fracture. This region is characterized by a darker, linear torn groove-like surface that contrasts with both the smooth notched area as well as the spongy appearance of the overload fracture (Fig. 2.4). To quantify the extent of the subcritical crack growth, the area fraction (area of subcritical cracking region divided by total area of fracture surface) is measured or the change in half-crack angle that results from the increased crack length from  $a_{mit}$  to  $a_{inst}$ .

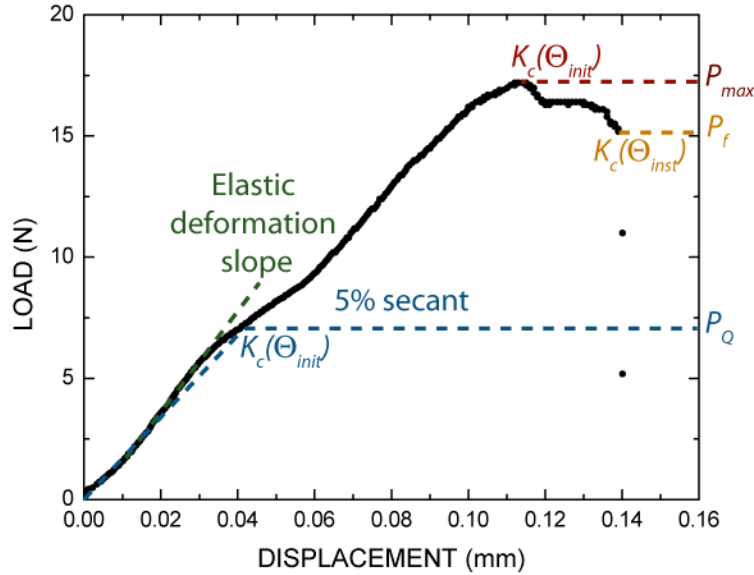


**Figure 2.5.** Representative load-displacement curve for a sharply-notched bend specimen. On the plot are the constructions for the determination of the loads  $P_Q$ ,  $P_{max}$ , and  $P_f$  used to compute the fracture toughness  $K_c$ .  $P_Q$  is given by the intersection of the loading curve with a line that has a 5% lower slope than the elastic deformation slope (5% secant construction),  $P_{max}$  is given by the maximum load, and  $P_f$  is given by the load at unstable fracture (instability). The loads are used with Eq. 12 to calculate the *crack-initiation*, *maximum load*, and *fracture instability* toughnesses, respectively. This figure is reproduced from Ref. 52

where  $P_c = P_Q$  and  $\Theta_c = \Theta_{init}$  for the *crack-initiation* method,  $P_c = P_{max}$  and  $\Theta_c = \Theta_{init}$  for the *maximum load* method, and  $P_c = P_f$  and  $\Theta_c = \Theta_{inst}$  for the *instability* method.<sup>ii</sup> This  $K_c$ -solution of Eq. 9 has a claimed accuracy of “a few %” for half-crack angles between 0 and 110°. <sup>50</sup>

The crack-initiation method will yield the lowest values, representing an intrinsic (no crack growth) toughness; this will be between 2 to 3 MPa√m for most types of bone, irrespective of orientation. The other two measures include some contribution from crack growth, which is where bone primarily derives its toughness<sup>54</sup>. As the *maximum load* procedure generally involves a higher load but a smaller crack size than *instability*, the difference in toughness values calculated using these two procedures will not be large; however, because the *instability* method uses a fracture load which corresponds *directly* to a known crack length, we believe that this approach provides a more appropriate and reliable measure of the single-valued  $K_c$  fracture toughness; additionally it incorporates contributions from both crack initiation and crack growth.

*Advanced measurements:* More elaborate procedures for evaluating the toughness of mouse femurs involve full R-curve measurements, which fully quantify the role of crack-

<sup>ii</sup> Ideally fracture toughness measurements should be independent of geometry. However, complete geometry-independence of the critical stress-intensity value is only really assured for crack initiation under plane-strain, small-scaling yielding conditions. By defining the toughness at instability after some degree of crack growth, the toughness value may thus become somewhat sensitive to the geometry under test (this incidentally is true for all R-curve measurements). In the present case, as the amount of stable crack growth is small, the effect of geometry will be minimal. Moreover, the most conservative approach is to use the SE(B) geometry, which is what was done here.

growth toughness, and  $J_c$  fracture toughness measurements, which incorporate the contribution from plastic deformation; in the latter case,  $K_c$  values can be back-calculated by noting that  $K_{c,eq} = (J_c E')^{1/2}$ . In principle, both measurements require accurate monitoring of crack extension and load-line displacement, which for small samples is best done with an *in situ* mechanical testing stage inside an environmental SEM (see Ref. 55); however, this may not be deemed to be a reasonable proposition for routine testing.<sup>iii</sup>

$J_c$  fracture toughness measurements can be made through using the same definitions of fracture criticality as used above for the  $K_c$  measurements, in terms of the initial and final crack sizes. Although relationships for the  $J$  are far less common than for  $K$ , one nonlinear elastic solution of relevance to bone is the edge-cracked cylindrical pipe solution, which was originally derived for the nuclear piping industry<sup>56</sup>:

$$J_{pl} = \alpha \sigma_0 \varepsilon_0 \pi R_m \left(1 - \frac{\Theta}{\pi}\right)^2 h_1 \left(\frac{M}{M_0}\right)^{n+1} \quad (13)$$

where  $\alpha$ ,  $\sigma_0$ ,  $\varepsilon_0$ , and  $n$  are determined from fitting the stress-strain curve to the Ramberg-Osgood constitutive relationship:  $\varepsilon/\varepsilon_0 = \sigma/\sigma_0 + \alpha (\sigma/\sigma_0)^n$ .  $M_0$  is given by:

$$M_0 = 4\sigma_0 R_m^2 t \left[ \cos\left(\frac{\Theta}{2}\right) + 0.5 \sin\left(\frac{\Theta}{2}\right) \right] \quad (14)$$

and  $h_1$  is the plastic geometric factor determined from tabulated values in Ref. 56. This solution is valid for  $0.5 > \Theta/\pi > 0$  and for  $20 \geq R_m/t \geq 5$ .<sup>56</sup> Eq. 13 defines the plastic component of  $J$ , whereas the elastic component is  $K^2/E'$ , as described above; the total  $J$  is then the sum of these two components. This solution, however, is only valid for thin-walled cylinders, specifically for  $R_m/t \geq 5$ , which limits its strict applicability to bones, in particular mouse femurs which tend to be more akin to thick-walled cylinders with  $R_m/t$  typically varying from 2 to 4. Currey has tabulated common values of  $R_m/t$  for a variety of animals and found that this ratio ranges from 1 to 4 for most land mammals;  $R_m/t$  only exceeds 5 for certain species of birds.<sup>57</sup> Unfortunately, the accuracy of the  $J$ -solution in Eq. 13 is not known for values of  $R_m/t < 5$ .

### **Chapter 2.2.3 – Structural evaluation of femora**

#### *Scanning Electron Microscopy*

In addition to the scanning electron microscopy (SEM) necessary to evaluate fracture toughness mentioned in the prior section, more fundamental evaluation of the structure of bone can be conducted via SEM. Portions of interest are isolated via low-speed saw, then the bone surface is polished with progressively finer grits of sand paper on a wet polishing station (down to 1200 grit). Then, a series of diamond polishing suspensions are used to achieve optimal smoothness. In this case, the first solution used

---

<sup>iii</sup> One advantage of the fracture instability measurement for  $K_c$  described above is that it effectively incorporates R-curve toughening during subcritical crack growth in the single-valued parameter, without the need for continuous crack monitoring. This definition of  $K_c$  is actually a steady-state fracture toughness, often associated with a “plateau” in the R-curve.

is a 1 $\mu\text{m}$  diamond suspension, then a 0.05 $\mu\text{m}$  diamond suspension to finish. This surface allows for not only detailed microscopy, which shows down to the lamellar (micron-scale) level, but also prepares the surface sufficiently for nanoindentation, which will be discussed in a future segment. With such a preparation, the samples can be observed in backscattering environmental SEM.

Backscattered electrons tend to bounce back at similar energies to the incident beam energy and reveal slight changes in topography better than secondary electrons which enter the sample, lose some energy, and are scattered back out of the sample. Additionally, this technique is very sensitive to atomic weight of the surface elements, since the incoming electrons whip around the nuclei of these surface elements and the number of electrons backscattered increases with increasing atomic number ( $Z$ ). As a result of this  $Z$  contrast, some of the contrast observed in this mode comes from varying degrees of mineralization. Brighter regions correspond to higher mineral content areas (more calcium,  $Z=20$ ) and darker regions correspond to lower mineral content areas (more carbon,  $Z=6$ ). These advantages allow for not only structural differences to be observed but also allow for some characterization of mineralization patterns via a quantitative back-scattering electron imaging (qBEI) technique.

#### *Quantitative Backscattered Electron Imaging*

As a result of the  $Z$  contrast observed in back-scattered SEM, the relative amounts of minerals can be quantified by a standardized technique called quantitative backscattered electron imaging, or qBEI. Roscher, et al., developed and validated the techniques used as part of this work.<sup>58</sup>

Carbon and aluminum are used as reference materials to calibrate the gray levels to known atomic numbers. The contrast and brightness of the instrument are adjusted such that the image from pure carbon corresponds to a gray level of 25 and the aluminum corresponds to 255. These two values are plotted on a graph of atomic number vs. gray-level. Two other reference materials, magnesium fluoride ( $\text{MgF}_2$ ,  $Z_{\text{mean}} = 10.17$ ) and fluoroapatite (FA,  $Z_{\text{mean}} = 14.43$ ) are scanned to verify that the contrast levels are set properly (all points on the atomic number – gray level plot will fall onto a single line).

Following this procedure, it is necessary to calibrate the gray level to a weight percent of calcium (wt% Ca). Two calibration materials are used. The first is a “zero level” Ca osteoid standard, which has between 0% and 0.17% wt% Ca. The second is a hydroxyapatite (HA) standard with 39.86 wt% Ca. The gray levels of each of these are plotted on a wt% Ca vs. gray level plot and connected with a standardization line.

At this point, the material of interest is scanned and gray level histograms are constructed. Then, the x-axis of the histogram is normalized such that the sum of the counts is 100% of the sample and the x-axis is converted to wt% Ca using the standardization curve made with the osteoid and HA. A weighted average of the wt% Ca gives a calcium concentration on the surface of the sample.

#### *Transmission Electron Microscopy*

The hierarchical nature of bone structure ranges from the nano-scale (collagen fibrils with thicknesses of 1.5nm) to the micro-scale (lamellae and osteocyte lacunae which have dimensions close to 7 $\mu\text{m}$ ) to the macro-scale (overall bone dimensions of millimetres or more). While traditional microscopy and SEM can probe the macro and

micro-scales, the resolutions are limited to a few microns. To investigate further, transmission electron microscopy, or TEM, is required.

Ultra-thin samples of bone are prepared to be electron-transparent, then a series of detectors collect electrons on the other side of the sample. A variety of contrast mechanisms are possible in such a setup. The easiest to interpret is mass or thickness contrast, which relies on thicker or more dense portions of the sample scattering more of the electrons than thin or less atomically massive portions. The second form of contrast stems from diffraction, which results from planes of atoms at various spacings scattering electrons at well-known angles, as computed by Bragg's law:

$$n\lambda = 2d \sin\theta \quad (15)$$

where  $d$  is the atomic plane spacing,  $\theta$  is the scattering angle,  $n$  is an integer, and  $\lambda$  is the wavelength of incident radiation. Another form of contrast is inelastic scattering, where the energy lost by electrons during their interaction with the sample will reveal the structure of the sample. Finally, phase contrast can arise from the phase of the electrons changing as a result of interaction with the sample.<sup>59</sup> Researchers investigating the nanostructure of bone have primarily relied on mass/thickness contrast to characterize the organization of collagen layers and lamellar structure,<sup>60,61,62</sup> which is consistent with the methodology employed in this work.

Transmission electron microscopy (TEM) was performed with a JEOL2000 TEM (JEOL Ltd.), operating at 120 kV, on specimens from the test groups to discern whether there were differences between the groups in the bone structure at sub-micrometer dimensions. Images were taken from the medial and lateral cortex near the fracture surface of each specimen. Specimens were fixed in anhydrous ethylene glycol for 24 hr, dehydrated by rinsing in 100% ethanol three times for 5 min in acetonitrile, and then infiltrated with resin (Agar Scientific) over several days. Mounting resin was prepared with 12 g Quetol, 6.5 g methyl nadic anhydride (MNA), 15.5 g nonenylsuccinic anhydride (NSA), and 0.7 g benzlydimethylamine (BDMA). The samples were agitated at room temperature in 1:1 solutions of acetonitrile and resin for 1 day, then 1:2 acetonitrile resin for 1 day, and finally 100% resin for 3 days under vacuum; the resin was changed every 24 hr. Samples were then cured in fresh resin for 24 hr at 60°C. Silver to gold sections (70–90 nm) were cut onto distilled water with an ultramicrotome using a 35 degree diamond knife. Samples were collected immediately on lacy carbon 300 mesh copper grids, and dried for 1 hr at 37°C.

### *Nanoindentation*

In an effort to quantify local structural changes, nanoindentation was performed on sectioned femora. Nanoindentation seeks to identify a local elastic modulus of an isotropic, well-understood solid. In this scenario, a sharp diamond indenter tip of known dimensions (in this case, a Berkovitch indenter) is pressed onto the surface of the solid and a load-displacement curve is collected from loading through unloading (Fig. 2.6).<sup>63</sup> An elastic modulus can be calculated from the area of the indentation,  $A$ , the Poisson's ratios of the indenter and sample (determined previously):

From Fig. 2.6,

$$S = \beta \frac{2}{\sqrt{\pi}} E_{eff} \sqrt{A} \quad (16)$$

where  $\beta$  is a constant of order 1,  $A$  is the area of the indent remaining on the sample after the indentation is complete, and  $E_{eff}$  determines the modulus of the sample in the following way:

$$\frac{1}{E_{eff}} = \frac{1-\nu^2}{E} + \frac{1-\nu_i^2}{E_i} \quad (17)$$

where  $\nu$  and  $E$  are the poisson's ratio of the sample and Young's modulus of the sample, respectively, and  $\nu_i$  and  $E_i$  are the corresponding values of the indenter.

This methodology is deceptively simple, however, one must be careful not to make erroneous assumptions. For example, as noted above, this technique is specific to isotropic materials of known structure. Bone is certainly not isotropic, but can be better described by transverse symmetry where a long axis is distinct from a transverse plane. Secondly, the simple nanoindentation technique assumes linear elasticity, whereas viscoelastic effects might more accurately describe bone, especially if different loading rates are considered. Finally, a highly heterogeneous three-dimensional structure such as bone may not respond to indentation as a homogenous linear elastic material might if, for example, holes or zones of changing modulus exist just beneath the surface which alter the observed modulus. As a result, many indentations need to be taken and averaged, which has been the case in many bone studies. Despite these efforts, it is important to take nanoindentation results of bone with some degree of skepticism, as the technique is

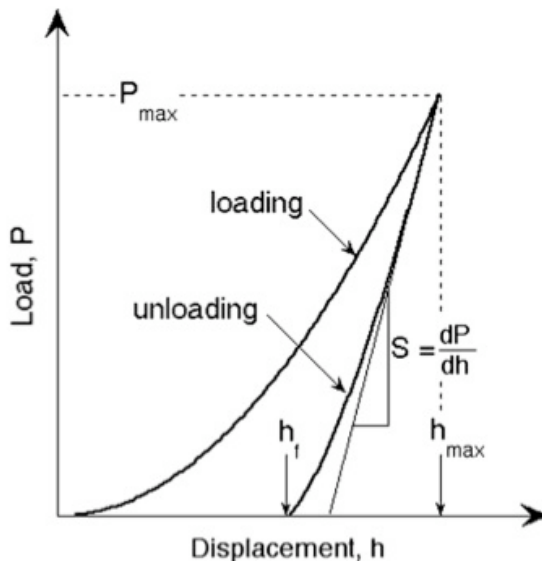


**Figure 2.6 Nanoindentation load-displacement curve.** From W. C. Oliver & G. M. Pharr, J Mater Res 19, 3 (2004).<sup>63</sup>

highly susceptible to operator choices as well as heterogeneous material which is not understood completely and may easily be affected inhomogeneously by externalities such as storage and other prior history. For reasons such as these, many qualifications must be made to the technique applied before one knows if the true Young's modulus was measured correctly. Some groups have made this effort by testing loading rates and holding patterns to avoid viscoelastic creep,<sup>64,65,66,67,68</sup> and despite these efforts, the true Young's modulus of bone may not be the result of such tests. Although interpretation of results may be sensitive to many factors, some of which may be unknown, nanoindentation may be used to compare elastic response of bone *within* a study between groups of

samples which underwent similar treatment. Thus, although the true Young's modulus may not be known for each sample, the relative increase or decrease of one group compared to another can be a reasonable claim to make.

Within this study, the following parameters were followed to compare cortical bone of mice which were obese to ones that were normal weight. Mouse femora were embedded in Buehler Epoxycure Resin epoxy and polished to 0.05  $\mu\text{m}$  with diamond polishing suspension. As drift may shift data over a long testing period, a quasi-static test is conducted. The loading rate is 100  $\mu\text{m/s}$  with a 10 s hold at the maximum load (600  $\mu\text{N}$ ). Stabilization of the tip at the maximum displacement is verified by inspection of the load vs. time data curve. Indents should be spaced around 5  $\mu\text{m}$  apart such that they do not interact with the plastic zone created by their neighbor, confounding results.

#### *X-Ray Microtomography*

As mentioned above, two-dimensional DXA techniques confound bone mineral content with bone size as the depth dimension of the bone cannot be measured. As a result, a three-dimensional technique was employed to measure a volumetric bone mineral density (vBMD). X-ray microtomography is a technique employing an x-ray source and a rotating sample, whereby two-dimensional scans are taken progressively through the depth of the sample, the bone mineral content is counted in each slice, then added together for all slices. The three-dimensional nature of the reconstructed slices allows for an average of the bone mineral density over a volume, resulting in a volumetric BMD.

In this study, X-ray micro-tomography (SR $\mu$ CT) was employed to measure the vBMD of all samples using synchrotron beamline 8.3.2 at the Advanced Light Source, Lawrence Berkeley National Laboratory. The three-dimensional resolution was 4.45  $\mu\text{m}$ . The samples were scanned in absorption mode at 14 keV and the reconstructed images were obtained using a filtered back-projection algorithm. The mean vBMD for each femur was calculated from a collection of the two-dimensional reconstructed slices.<sup>69</sup>

### **Chapter 2.3 – Statistics**

Throughout the study, measured values are presented as mean  $\pm$  standard deviation. Two-tailed independent sample Student's T-tests were executed to determine differences in measured variables between the Chow and HFD groups (SPSS 15.0, SPSS Inc). Differences were considered to be significant at  $P < 0.05$ .

Correlation analysis was performed within each group (Chow and HFD) to identify trends that might be diet-independent. To mitigate the risk of Type I errors, related measurements that were highly and positively correlated were grouped together and given a composite score (sum of Z-scores). Comparison of Z-scores allows for the standardization of scale for the groups being compared and also allows for the combination of related measurements to be grouped into one composite group. As an example, since yield strength, maximum strength, and bending modulus are all measured using the same test, it makes sense to make a composite "bone strength" measure which adds the Z-scores for the three separate measures for each sample tested. It is also evident that the yield strength – bone size relationship might be similar to the maximum



strength – bone size relationship due to the fact that they stem from the same mechanical test, hence the combination of yield strength and maximum strength makes for a cleaner picture of relationships in the statistical analysis. For those measures which do not correlate to similar measurements ( $P_y$ ,  $P_u$ ) or were conceptually unique ( $K_c$ , vBMD), the Z-score for that measurement was used in the analysis without any modification. Correlation analysis was performed between scores of predictive measures (mineral density, composite bone size score and two body composition measures) and mechanical property outcomes (composite strength and modulus score, fracture toughness and two load measures). The correlation between yield and maximum loads was weak, so these were not combined into a composite.

### Chapter 3 – Effects of Obesity on Cortical Bone in Young Mice

This chapter discusses the effects of diet-induced obesity on young mice, which are expected to have reduced fracture risk compared to the fracture risks observed in obese children and adolescents. To clarify the effects of HFD on the mechanical properties and microstructure of bone, femora from C57BL/6 mice fed either a HFD or standard laboratory chow (Chow) were evaluated for structural changes and tested for bending strength, bending stiffness and fracture toughness. In young obese high fat fed mice all geometric parameters of the femoral bone, except length, are increased but strength, bending stiffness and fracture toughness all are reduced. This increased bone size and reduced size-independent mechanical properties suggests that obesity leads to a general reduction in *bone quality* despite an increase in *bone quantity*; yield and maximum loads, however, remained unchanged, suggesting compensatory mechanisms. It is concluded that diet-induced obesity increases bone size and reduces size-independent mechanical properties of cortical bone in young mice. This study indicates that bone quantity and bone quality play important compensatory roles in determining fracture risk.

## Chapter 3.1 – Childhood obesity and fracture risk

As discussed in Chapter 1, children and adolescents tend to have higher fracture risk when they are overweight or obese compared to their normal-weight peers. Taylor, *et al.* found greater musculoskeletal discomfort, joint misalignment, and fracture incidence in obese adolescents compared to non-obese individuals.<sup>15</sup> Also since discomfort and reduced mobility are more prevalent in overweight adolescents, less exercise is likely and therefore childhood obesity makes it more likely that obesity will persist into adulthood. In addition to the increased fracture incidence, Leonard, *et al.* found increased spinal aBMD, spinal BMC, and whole body BMC in overweight adolescents. Whole body BMC indicates a larger skeleton, and indeed, the overweight children were taller and had larger bones overall than their normal weight peers.<sup>70</sup> These findings suggest that larger bone size is not sufficient to reduce fracture incidence, and therefore it is possible that such considerations as the structure of the bone tissue and hormonal interactions with bone formation may be important in determining and predicting fracture risk more accurately.

This first study investigates the effects of obesity on cortical bone in young mice. This is achieved by considering changes in bone size, tissue quality as defined by tissue mechanical properties, and structure. Specifically, size-dependent and size-independent material properties are measured to distinguish tissue behavior from whole-bone behavior. The changing levels of relevant hormones (i.e. leptin and IGF-I) are also considered in trying to explain how a whole-body response to excess body fat can change bone structure and behavior. All methodologies employed here were described in detail in Chapter 2.

## Chapter 3.2 – Results of High-Fat Diet-Induced Obesity on Young Mice

### *Chapter 3.2.1 – Metabolic Phenotype of Experimental Animals: Validation of Obesity Model*

To explore the effects of obesity on cortical bone, mice were fed a high-fat diet (HFD) for 19 weeks (top mouse, Fig. 3.1a). As shown in Figure 3.1b, HFD mice gained weight twice as fast as the Chow (control) group ( $n = 15$  in each group). Both groups stopped gaining weight after week 18 (week 14 of the diet); mean weights stabilized at  $34.7 \pm 2.1$  g for the Chow group and  $47.3 \pm 3.4$  g for the HFD group. DXA analysis revealed that HFD mice had 98% more fat mass than Chow mice ( $P < 0.001$ ) (Fig. 3.1c), but showed similar lean mass. As expected, the serum leptin concentration was significantly increased by the high-fat diet. The HFD group had 385% higher serum leptin concentration than in Chow ( $P < 0.001$ ) (Fig. 3.1d). Also, IGF-I levels were increased significantly in the HFD group ( $P < 0.01$ ); the HFD group showed a 34% increase in serum IGF-I concentration compared to Chow (Fig. 3.1e). Increased weight, fat mass, and serum concentrations of leptin and IGF-I confirm that the high-fat diet provides a successful model of obesity for the current study.

Blood glucose levels indicated that hyperglycemia developed within the last week or so of the study, which is unsurprising in diabetes-prone C57Bl6 mice, but this diabetic

condition was not present throughout most of the length of the study. Details of the blood glucose tests are discussed in Appendix E.

### ***Chapter 3.2.2 – Bone Densiometry Studies***

To understand the effects of obesity on cortical bone in mice, it is critical to compare bone-mineral content and density between test groups. As shown in Figure 3.2a, BMC levels were 7.5% higher in HFD mice than in Chow mice ( $P < 0.001$ ), consistent with their increased bone size. Although the total amount of bone was larger, the whole-body areal bone mineral density (aBMD), measured using DXA, was not significantly different between the Chow and HFD groups (Fig. 3.2b). Further evaluation of the DXA data revealed that spinal BMC and aBMD did increase significantly with weight, but that femoral BMC and aBMD were unchanged in the HFD group (Figs. 3.2c, 3.2d, 3.2f, and 3.2g, respectively). As mentioned in Chapter 2, DXA is limited to a two-dimensional approximation of a three-dimensional distribution of mineral within bone. It especially suffers from a confounding of bone size with mineral content. As a result, synchrotron tomography was used to evaluate the volumetric bone mineral density (vBMD) of the femoral cortex to understand the three-dimensional mineral distribution of the femur only. This yielded a similar result, with no significant difference between the Chow and HFD groups (Fig. 3.2e); this is consistent with prior reports that lean body mass, rather than fat mass, is more predictive of BMD.<sup>30,32,33,71</sup>

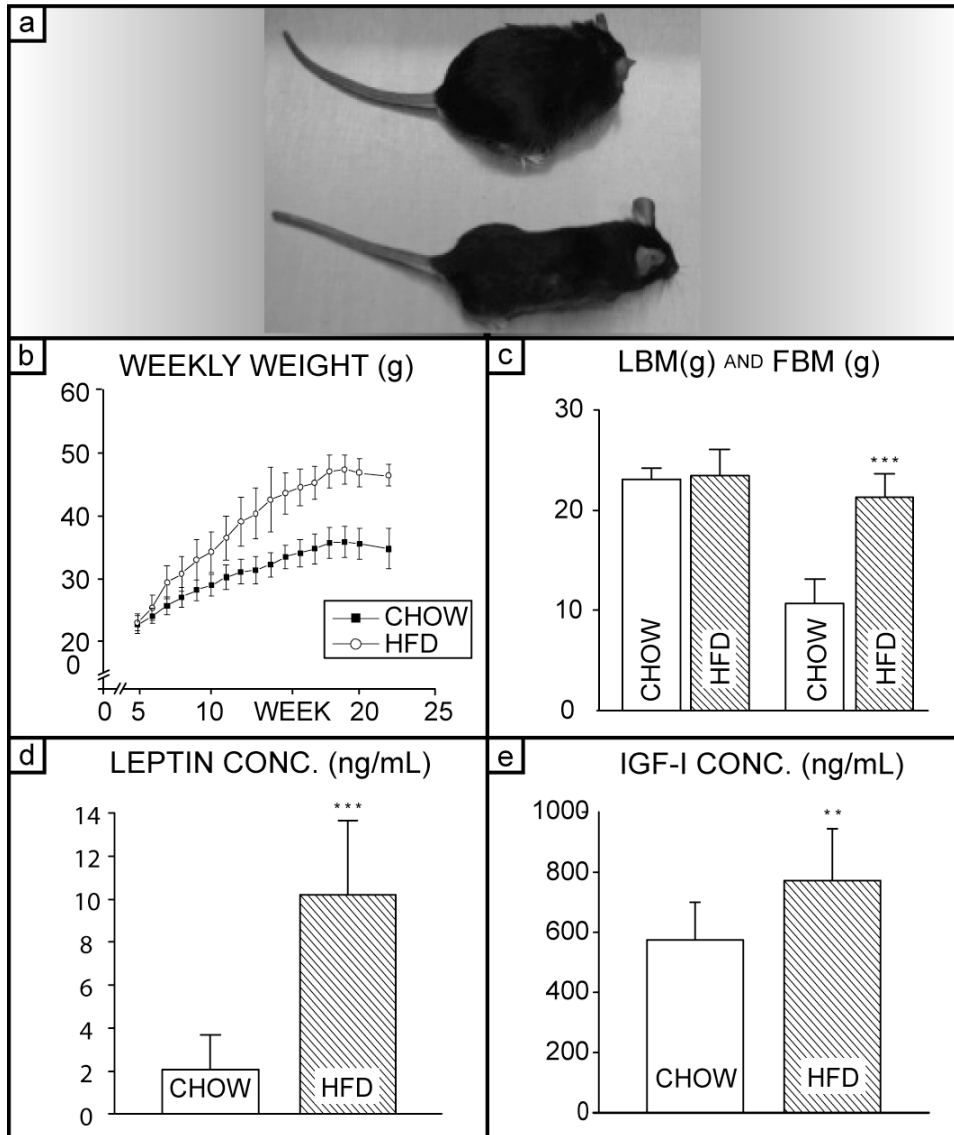


**Figure 3.1. Validation of Obesity Model: Body Composition, Serum Leptin Concentration, and Bone Mineral Measures.** (a) Representative HFD and Chow mice. Typical HFD mouse (top) and typical Chow mouse (bottom) at the conclusion of the 19 week diet period; (b) Average weekly weights of Chow and HFD groups. Horizontal axis is mouse age in weeks; (c) lean body mass (left) and fat body mass (right) for Chow and HFD groups at conclusion of study; (d) serum leptin concentration at conclusion of study; (e) serum IGF-I concentrations at the conclusion of study. No difference was observed in lean mass, but significant increase in the fat mass and in leptin concentration for the HFD group.  $n=15$  for the Chow group and  $n=14$  for HFD group. (\*  $P<0.01$ , \*\*\*  $P<0.001$ ). Reproduced from Ref. 72.

### ***Chapter 3.2.3 – Bone geometry changes as a result of high-fat diet***

Since bone geometry can have a significant impact on the macro-mechanical behavior of cortical bone,<sup>73,74,75</sup> several bone geometry parameters were measured; data are summarized in Figure 3.3. With the exception of bone length, all size parameters from the HFD group were significantly larger. Cortical wall thickness (Ct.Th.) was increased by 10.5% ( $P = 0.012$ ), outer cortical radius ( $R_o$ ) by 6.1% ( $P = 0.005$ ), inner cortical radius ( $R_i$ ) by 4.8% ( $P = 0.027$ ), cortical cross-sectional area (Ct.X-Sect.A.) by 11.4% ( $P = 0.009$ ), and the second moment of area (M.A.) by 26.7% ( $P = 0.004$ ). Overall, there was a clear increase in bone size with diet-induced obesity.

### ***Chapter 3.2.4 – Mechanical testing: evaluation of tissue quality via size-independent mechanical measures and whole-bone behavior via size-dependent measures***

To evaluate the quality of the cortical tissue, size-independent mechanical properties were measured. Additionally, size-dependent properties, which are an indication of the load-bearing ability of cortical bone, were also determined. Mechanical test data are summarized in Figure 3.4. Size-independent parameters which indicate the inherent mechanical properties of the tissue, specifically bending strength, bending stiffness and fracture toughness, were all lower in the HFD group than in the Chow group. Bone in the HFD group displayed 24% lower yield strengths ( $\sigma_y$ ,  $P < 0.001$ ), 15% lower maximum strengths ( $\sigma_u$ ,  $P = 0.012$ ), 19% lower bending stiffness ( $E$ ,  $P = 0.017$ ), and 13% lower fracture toughness ( $K_c$ ,  $P = 0.027$ ). Based on the increased BMC, a decrease in the measured strains for yielding and fracture might be anticipated; however, no changes were observed in yield or maximum strains ( $\epsilon_y$ ,  $\epsilon_u$ ); these parameters are geometry-sensitive as strain is proportional to the outer bone radius). The size-dependent mechanical property measurements of yield load ( $P_y$ ) and maximum load ( $P_u$ ), which are indicative of the load-bearing capacity of the actual bone, also did not change significantly. The reduction in size-independent mechanical properties in the HFD group indicates that the quality of the bone tissue is reduced, despite its increased size.

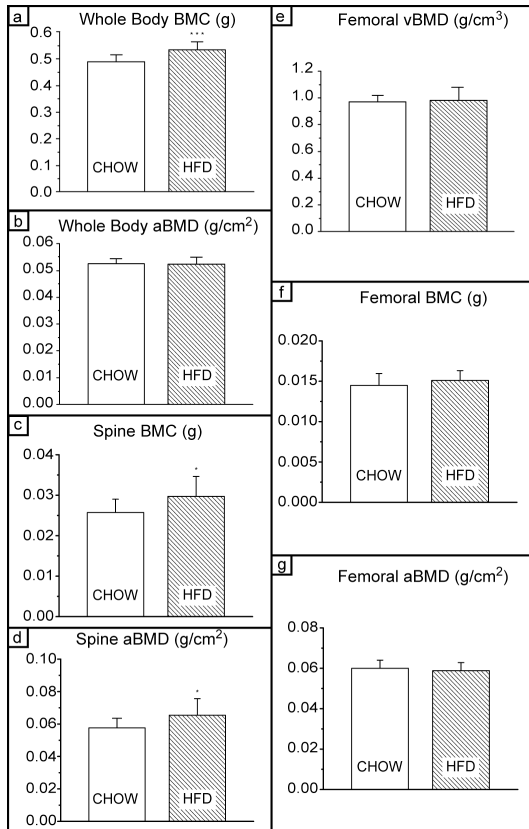


**Figure 3.2. Bone quantity measures – Bone mineral** (a) Whole-body bone mineral content (BMC); BMC is higher in the HFD group, which is expected because bones are larger (\*\* $P < 0.001$ ). (b) Whole-body areal bone mineral density (aBMD) is unchanged, which is not surprising as the lean body mass was unchanged (see Fig. 1). (c) Bone mineral content of the spine and (d) areal bone mineral density of the spine are significantly higher as a result of HFD (\*  $P < 0.05$ ). (e) volumetric bone mineral density (vBMD) of the femoral cortical bone as well as (f) femoral BMC and (g) are not significantly different between groups. Reproduced from Ref. 72

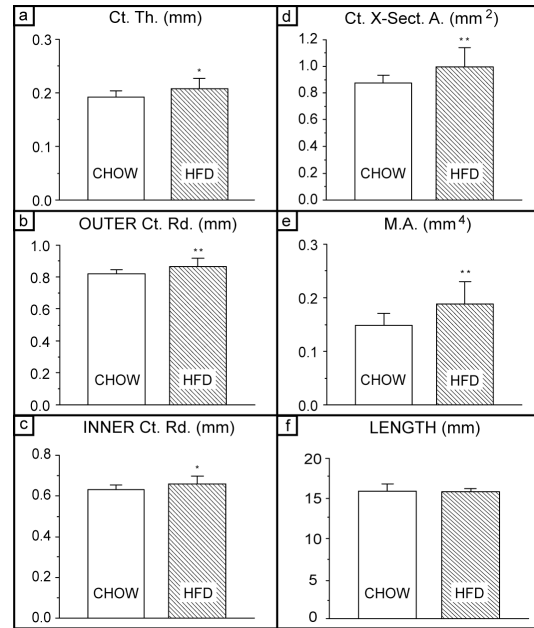


**Figure 3.3. Cortical bone quantity measures – Bone size:** (a) Average cortical thickness; (b) outer cortical thickness; (c) inner cortical radius; (d) cortical cross-sectional area; and (e) second moment of area. Significant increase (\*  $P < 0.05$ ; \*\*  $P < 0.01$ ) for the HFD group is observed for all measures except (f) femoral length. (g) Whole-body bone mineral content (BMC); BMC is higher in the HFD group, which is expected because bones are larger (\*\* $P < 0.001$ ). (f) Whole-body areal bone mineral density (aBMD); and (i) volumetric bone mineral density (vBMD) of the femoral cortical bone are not significantly different between groups, which is not surprising as the lean body mass was unchanged (see Fig. 1).  $n = 15$  for the Chow group and  $n = 14$  for HFD group. Reproduced from Ref. 72.

**Chapter 3.2.5 – Structural characterization: mineral organization and lamellar alignment of cortical bone**

The mechanical testing suggested that the quality of the bone matrix is affected by the HFD condition. This was further assessed by scanning (SEM) and transmission (TEM) electron microscopy. SEM images indicate that the orientation of osteocyte lacunae and the lamellar structure, are less ordered and aligned in the HFD group (Fig. 3.5). Corresponding TEM images from the Chow and HFD mouse cortical bone are shown in Figure 3.6. In the Chow group, the bone was well aligned and appeared to be well organized (Fig. 3.6a); the HFD group displayed poorer mineral organization (Fig. 3.6b). Diffraction patterns taken from several regions were indexed to correspond to hydroxyapatite in both groups. Diffraction patterns (not shown) taken from the Chow group more frequently displayed characteristic (002) plane arcs related to oriented bone, confirming that the mineral organization was greater in normal bone than HFD bone.

Quantitative backscattered electron imaging (qBEI) investigations did not yield differences in the weight percentage of calcium for the two groups in any of the four physiological locations investigated (posterior, medial, anterior, and lateral) nor were the averages for the whole cross-sectional samples evaluated. All calcium weight percents ranged from 26.2 to 28.3 with no statistical differences between groups. Although no differences are observed in the calcium content of the bones, this measurement does not account for the distribution of calcified regions or the ordering of the structure. So, although two samples might have identical

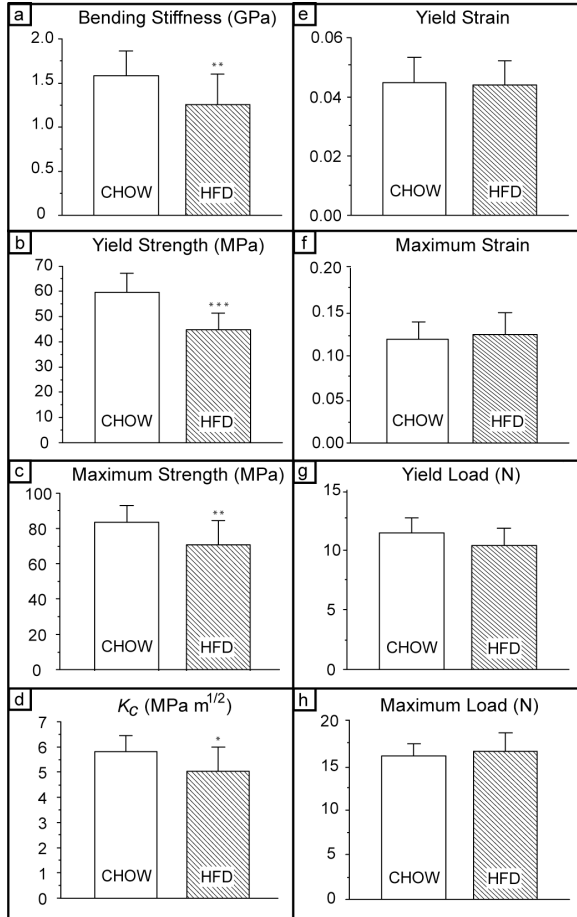


**Figure 3.4. Cortical bone quality: whole-bone and tissue-level mechanical property measurements:** (a) Yield strength; (b) maximum strength; (c) bending stiffness; (d) fracture toughness,  $K_C$ ; (e) yield load; (f) maximum load; (g) yield strain; and (h) maximum strain. Measured size-independent mechanical properties (except strain) were significantly decreased for HFD group vs. Chow group despite increased bone size (a-f); these parameters are an indication of bone-tissue quality. Size-dependent measures which address whole-bone behavior (specifically, load) did not differ between groups indicating a compensatory mechanism between bone size and tissue quality.  $n=15$  for the Chow group and  $n=14$  for HFD group (\*  $P<0.05$ ; \*\*  $P<0.01$ ; \*\*\*  $P<0.001$ ). Reproduced from Ref. 72.



weight percents of calcium, the organization within the two samples may vary significantly and therefore the quality of bone may still be different. These differences are highlighted mostly in the TEM results.

Nanoindentation evaluation at posterior, medial, anterior, and lateral portions of the mid-diaphysis did not yield any significant differences between the groups. All moduli measured were in the 30-35 GPa range. No significant changes were observed when all indents were averaged over a bone sample to approximate whole-bone modulus. As discussed in Chapter 2, nanoindentation does not correspond well with whole-bone behavior due to local heterogeneities. One might, however, conclude that on the size-scale of the indentation, the material response was unchanged by the high-fat diet and that the changes really take place at higher length scales. This argument does conflict with TEM results, however, which show decreased structural quality down to the micron scale. In general, nanoindentation results in this case do not seem to provide additional information beyond that provided by the combination of structural analysis and whole-bone mechanical testing.

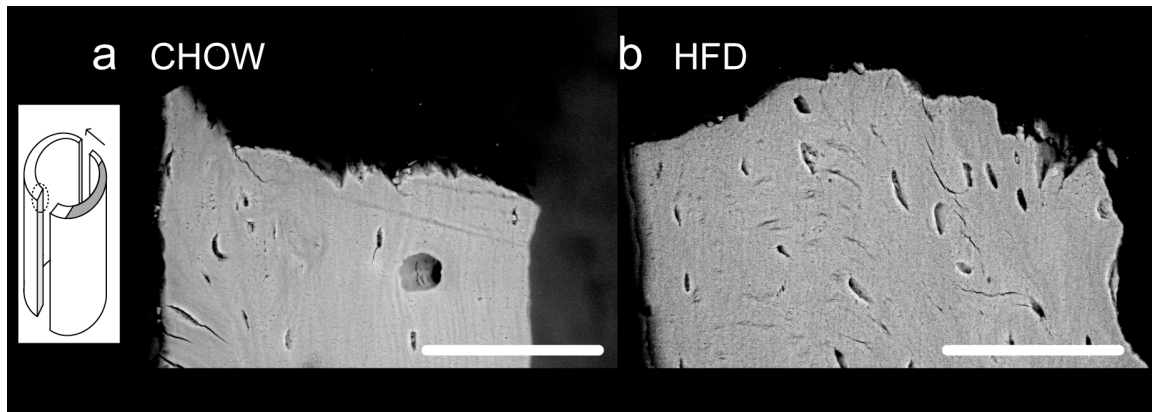


**Figure 3.5. Through-wall SEM images of fracture region showing tissue structure at the whole-bone scale. (a) Cortical wall in bone from Chow group; (b) Cortical wall in HFD group. The scale bar indicates 100  $\mu\text{m}$ . The medial cortex in HFD bone (b) shows reduced alignment of osteocyte lacunae and reduction in lamellar alignment at the tissue level. These images are representative of five samples each of HFD and Chow. The inset indicates that images were taken from vertical sections through a region beyond the notch at the crack surface. The dark grey region indicates the notch, and the arrow indicates direction of crack growth, with crack propagation happening evenly from both sides of the notch. Reproduced from Ref. 72.**

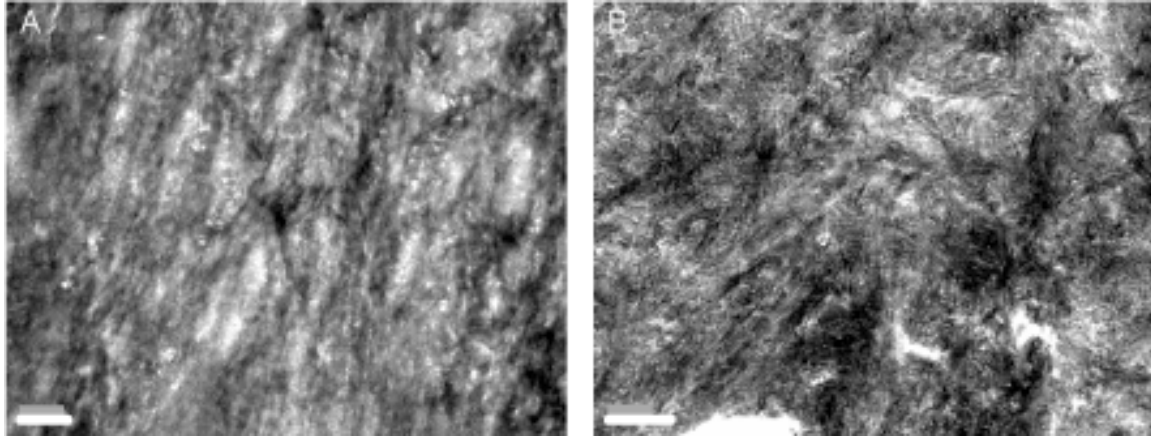


**Figure 3.6. High-magnification TEM images of structure and mineral organization.** (a) Mineral organization of bone from Chow group; and (b) mineral organization of bone from HFD group. The scale bar indicates 200 nm. Mineral appears more poorly aligned and organized in HFD bone than in Chow bone, suggesting a reduction in microstructural tissue quality. Reproduced from Ref. 72.

### ***Chapter 3.2.6 – Correlation Analysis***

In order to evaluate relationships between bone size, mechanical properties, and body composition, correlation analyses were performed between scores for each measure; correlation coefficients and corresponding  $P$ -values are summarized in Table 1 (Q-Q analysis revealed that the data were normally distributed). In both Chow and HFD groups, bone-size measures have the highest correlation coefficients with size-independent mechanical measures, although significance was more difficult to achieve in the Chow group due in part to the smaller variances within this group. In the Chow group, vBMD was correlated positively with fracture toughness ( $K_c$ ), and fat body mass (FBM) was correlated negatively with maximum load ( $P_u$ ). In HFD group, lean body mass (LBM) was correlated negatively with strength and bending modulus. It was also found that LBM is positively correlated with bone size measures, and FBM is weakly negatively correlated with bone size measures (Table 1).

Overall, a trend of decreasing mechanical properties with concurrent increase in bone size is apparent in the correlation analysis, but it is unclear at this time whether bone-size changes lead to bone-tissue quality changes and vice versa, or whether size and tissue quality change simultaneously. In this respect, further study is needed to determine whether this is a causal or correlative relationship.

Predictors	a. Chow (n=15)				b. HFD (n=14 <sup>†</sup> )			
	Size – independent measures		Size – dependent measures		Size – independent measures		Size – dependent measures	
	$(\sigma_y, \sigma_u, E)$	$K_c$	$P_y$	$P_u$	$(\sigma_y, \sigma_u, E)$	$K_c$	$P_y$	$P_u$
vBMD	0.12	0.55*	0.08	-0.42	-0.24	-0.07	0.24	-0.01
(M.A.,A,R <sub>o</sub> )	-0.44	-0.43	0.23	0.19	-0.86***	-0.59*	0.57	-0.04
LBM	-0.37	-0.18	0.25	-0.07	-0.67*	-0.16	0.50	0.02
FBM	-0.30	0.16	-0.11	-0.53*	0.41	0.10	-0.54	-0.02
	c. Bone size in Chow- (M.A.,A,R <sub>o</sub> )				d. Bone size in HFD - (M.A.,A,R <sub>o</sub> )			
LBM	0.514*				0.548			
FBM	-0.215				-0.315			

<sup>†</sup> One mouse was found to be diabetic and was excluded from all analyses.

\* $P < 0.05$

\*\* $P < 0.01$

\*\*\* $P < 0.001$ .

vBMD = volumetric bone-mineral density; M.A.= second moment of area; A = Ct. cross-sectional area; R<sub>o</sub> = outer Ct. Rd; LBM = lean body mass; FBM = fat body mass;  $\sigma_y$  = yield strength;  $\sigma_u$ = maximum strength; E = bending modulus;  $K_c$  = fracture toughness;  $P_y$ = yield load;  $P_u$ = maximum load. (M.A., A, R<sub>o</sub>) = composite bone size score,  $(\sigma_y, \sigma_u, E)$  = composite strength and modulus score.

**Table 1. Correlation coefficients between standardized properties in bone from (a), (c) Chow and (b), (d) HFD groups.** Coefficients from correlation analysis applied between standardized mechanical properties and standardized bone and physiological properties of (a) Chow group and (b) HFD group. In cases where measurements were related and highly positively correlated, a composite score was used in the analysis. Bone size is the largest predictor of mechanical properties, more so than bone-mineral measures or body composition. Interestingly, size-independent measures of bone quality are most affected by the size of the bone, which implies a reduced quality with increasing quantity. Correlation coefficients between body mass measures and bone size measures show that LBM is positively correlated with bone size in both groups (c) & (d), and that FBM is very weakly negatively correlated with bone size. HFD (d) was almost significant for LBM-bone size correlation ( $P=0.053$ ).

### Chapter 3.3 – Discussion of Young Mouse Results

It is clear that a high-fat diet leads to obese mice with enhanced bone quantity (larger bone size and mineral content) but with diminished bone quality (lower size-independent mechanical properties) as compared to bone from mice on a standard Chow diet. Interestingly, while the (size-independent) bone stiffness, strength and toughness clearly deteriorated due to the high-fat diet, the yield and maximum loads that the femurs could sustain prior to failure were essentially unchanged by diet. Indeed, in terms of the loads the bones can withstand, the increase in bone size in the HFD group occurred to the extent necessary to maintain a given load-bearing capability. This argument supports the hypothesis that bone adapts to maintain the optimal size and material properties for a particular set of normal, or daily, physiological conditions, deemed “customary loading” by Turner.<sup>36</sup> Once a certain balance has been reached between these customary loads and the amount of bone necessary to support these loads, no more energy is expended in improving bone quality, a notion supported by Turner in his discussion of threshold behavior for remodeling activation in bone.

In addition to loading, hormones play an important role in bone response to obesity. Leptin, which controls body weight, reproduction and bone remodeling, is secreted by adipocytes and is found in higher concentrations in the obese. Its actions in bone are discussed in detail by Karsenty and references therein.<sup>40</sup> Whether leptin’s specific effects are beneficial or antagonistic to bone quality is under debate,<sup>71,76,77,78,79,80,81,82</sup> although there is some consensus that increased leptin production in humans is associated with higher bone mineral density and bone size.<sup>9</sup> A proposed mechanism for this action is posited by Baldock and others whereby increased leptin production inhibits the action of neuropeptide Y (NPY) in the hypothalamus. As NPY is a potent inhibitor of bone growth, its inhibition by the presence of increased leptin production is consistent with increased body weight and bone size, especially increased periosteal circumference of long bones.<sup>83,84</sup> Finally, increased bone size, especially the periosteal circumference, as well as increased body weight have been associated with increased serum concentrations of IGF-I.<sup>37,38</sup> Significant increases in serum IGF-I for the HFD group are observed, which could explain at least some of the increased bone size, although this was not explored as a possible causation in this study.

It should also be noted that the mice in this study were young (4 weeks) at the beginning of the study. The reduction of quality of bone tissue despite increased body weight is in agreement with clinical observations that adolescents and children have increased bone fracture incidence with obesity.<sup>15</sup> Whether the qualitative effects would be seen in adult mice is discussed in Chapter 4. It is postulated that increases in bone size with obesity would be observed in adult or aged mice. Reduced fracture incidence in adults suggests that the qualitative reduction seen in adolescent animals would be lessened in adults. Furthermore, the observation that LBM is positively correlated with bone size measures (Table 1) are also consistent with prior studies looking into independent effects of lean body mass and fat body mass on bone size in adolescents.<sup>30,81,85</sup> Together, these similarities point to consistency between animal studies and observations in large human cohorts and also reveal the need for additional studies to investigate the progression of bone health with obesity.

It is conceivable that the effects of this study could be attributed to an increased rate of bone growth in the HFD group or to dietary choice. It is shown that bone indeed grew faster in the HFD group, as the bone size in this group is larger than that in the Chow group after a similar length of study, although changes in growth rates between groups are not directly measured. It is possible the HFD femora grew to accommodate accumulating weight faster than the system can optimally support, thereby resulting in poorer quality bone. This behavior of rapid bone deposition to support weight gain is well known in woven bone in the long bones of livestock that need to walk soon after birth. Additionally, it has been observed that bone growth rates affect bone microarchitecture in birds<sup>86</sup> and many other animals. It is widely accepted that rapidly growing bone will be of inferior structural quality to that of more slowly grown bone<sup>57</sup> although further study could illuminate more specific growth rate–structure relationships, especially if rapidly growing animals such as high-growth, or *hg*, mice are compared to controls. SEM images showing differences in the apparent structural quality of bone in obese mice compared to the Chow group (Fig. 3.5) lend some credence to this hypothesis; TEM images also suggest a reduction in material quality with concurrent increase in weight (Fig. 3.6).

In examining whether the observed effects are due to obesity and not simply diet quality, standardized correlation analysis (Table 1) for the Chow and HFD groups suggest that diet choice is not the sole cause of the effects observed. This follows from the regression data where the general trends that exist in the overall study (in HFD *vs.* Chow groups) are also found within the individual groups. For example, the negative correlations between size-independent mechanical behavior and bone size are observed within both the Chow and HFD groups. Most interestingly, larger bones are consistently associated with poorer mechanical properties, independent of the obesity condition. This implies that larger bones in obese individuals are not necessarily protective against fracture, a fact which is supported by similar yield and maximum loads between the two groups. Since bone size increases and mechanical property decreases seem to be occurring concurrently, and are both brought about by obesity, bone size and size-independent mechanical properties are linked in the correlation analysis of this work.

It is noted the presence of a hyperglycemic state in the majority of the HFD mice within the last week of the study. While the diabetic condition did not persist throughout our study, as indicated by the fasting blood glucose levels at age 15 and 21 weeks, it did appear to come into play by age 22 weeks, as indicated by the fasting blood glucose levels of the glucose tolerance test. Diabetics are known to have increased fracture risk, which is consistent with the results presented here, and it is possible that the hyperglycemia played a role in the results observed. The specific role of hyperglycemia was not investigated as part of this study; however, the short length of time that hyperglycemia was present in the obese mice makes it an unlikely candidate as the *sole* contributor to the effect seen.

In conclusion, this study has shown that diet-induced obesity in mice increases bone size yet decreases the (size-independent) mechanical properties of cortical bone. The maximum loads that the bones can sustain, however, remain essentially unchanged with the implication that the quality and quantity of bone act in a compensatory manner to optimize the load-bearing behavior of bone.

## **Chapter 4 – Changes in Cortical Bone Response to High-Fat Diet from Adolescence to Adulthood in Mice**

This chapter discusses the response of cortical bone to high-fat diet in young and adult mice in order to gauge age effects. Obese children and adolescents tend to have increased fracture risk, whereas adults tend to have the reverse trend. To clarify the effects of HFD on the mechanical properties and microstructure of bone, femora from two age groups of C57BL/6 mice fed either a HFD or standard laboratory chow (Chow) were evaluated for structural changes and tested for bending strength, bending stiffness and fracture toughness. The results indicate that both young and adult obese high fat fed mice strength, bending stiffness, and fracture toughness are all dramatically reduced while bone size response changes from young to adult. Microstructural deficiencies also point to reduced structural quality in both age groups. Calcein investigations indicate that the bone response to obesity shifts from the periosteum to the endocortex with age. In support of that shift, IGF-I is significantly increased for young only implying increased periosteal activity whereas adults show no change. It is concluded that despite human fracture trends, adult mice seem to be just as at risk for bone fracture, if not more so, than the young group although cortical bone in the two age groups responds to obesity differently.

## Chapter 4.1 – Fracture risk in adults versus adolescents

As discussed in Chapter 1, adults tend to have decreased fracture risk with obesity,<sup>5,6,7,8,9,10,11,12</sup> whereas children and adolescents tend to have the reverse trend.<sup>15,41</sup> In adults, increased bone mineral density has been reported,<sup>5,6,7,8,9,10,11,12</sup> which many have cited as the primary reason for the observed reduction in fractures. In adolescents, there are developmental aspects such as muscle development and posture control in adolescents,<sup>16,17,18</sup> as well as diseases such as diabetes.<sup>42</sup> It should be noted that fracture risk in adults with type-2 diabetes does tend to increase in adults<sup>41</sup> and although fracture rates of diabetic children have not been reported, reduced bone mineral content and bone size have been observed in type 1 diabetic adolescents, which does imply an increased fracture risk.<sup>42</sup>

These observations indicate changes in response to obesity with age, which are considered here by studying two groups of wild-type mice: a young group and an adult group. The varying fracture rates reported in public health studies would imply that adult cortical bone tends to have a more favorable response to increased adiposity than young cortical bone, although complicating factors such as diabetes and other diseases may change the overall fracture risks reported by these studies.

In addition to evaluating serum leptin and IGF-I concentrations as in the first study (Chapter 3), non-enzymatic glycation and calcein labeling are considered in this study. The association of increased AGEs with decreased fracture toughness<sup>43,44,45</sup> could help to explain some of the observed results. Higher AGEs would also be a logical consequence of a high-fat diet, which should increase blood glucose levels, to subsequently increase the rate of NEG. Additionally, calcein labeling allows for the determination of bone growth activity near the end of the experiment.

Primarily, mechanical effects are considered. To fully understand the mechanical integrity of the tissue, size-independent measures such as maximum and yield stress, bending modulus, and fracture toughness are conducted. Structural changes, such as larger bone size, have been observed with obesity<sup>32,70,79,85</sup> and are an important characteristic to evaluate in investigating the effects of obesity on bone and fracture risk. Beyond macroscopic dimensional changes such as femoral length and circumference at the midshaft, bone growth rates and qualitative imaging provide further insight into the investigation. By combining mechanical testing, biological factor consideration, and structural evaluation, this study aims to address how obesity affects cortical bone at two stages in life, adolescent and adult, in an effort to further understand how fracture risk may develop throughout life. All methodologies employed here were described in detail in Chapter 2.

## Chapter 4.2 – Results of High-Fat Diet-Induced Obesity on Young and Adult Mice

### Chapter 4.2.1 – Metabolic Phenotype of Experimental Animals: Validation of Obesity Model

In order to evaluate the effects of obesity, it is imperative to investigate whether the diet model has successfully produced obesity in the test groups. Figure 4.1 summarizes the results of the weight and hormone changes in this study. Both HFD groups were significantly heavier than their Chow counterparts, with aHFD being 52.7% heavier than aChow and yHFD being 44.2% heavier than yChow. Unsurprisingly, fat body mass (FBM) increased by 192% and 229% in adults and young HFD, respectively, compared to aChow and yChow. Lean body mass (LBM) did change slightly (increased by 15% in each group), but this change was significant so it is likely a contributing factor to the results observed.

Blood glucose tests indicated that the obese groups were likely diabetic. Blood glucose levels in the obese groups were double the levels in the normal groups ( $191.9 \pm 41.1$  mg/dl in aHFD vs.  $99.4 \pm 29.8$  mg/dl in aChow,  $P < 0.001$ ;  $187.7 \pm 39.1$  mg/dl in yHFD vs.  $97.7 \pm 16.3$  mg/dl in yChow,  $P < 0.001$ ). This result is not surprising as C57Bl/6 is known to be easily susceptible to diabetes on high-fat diets.

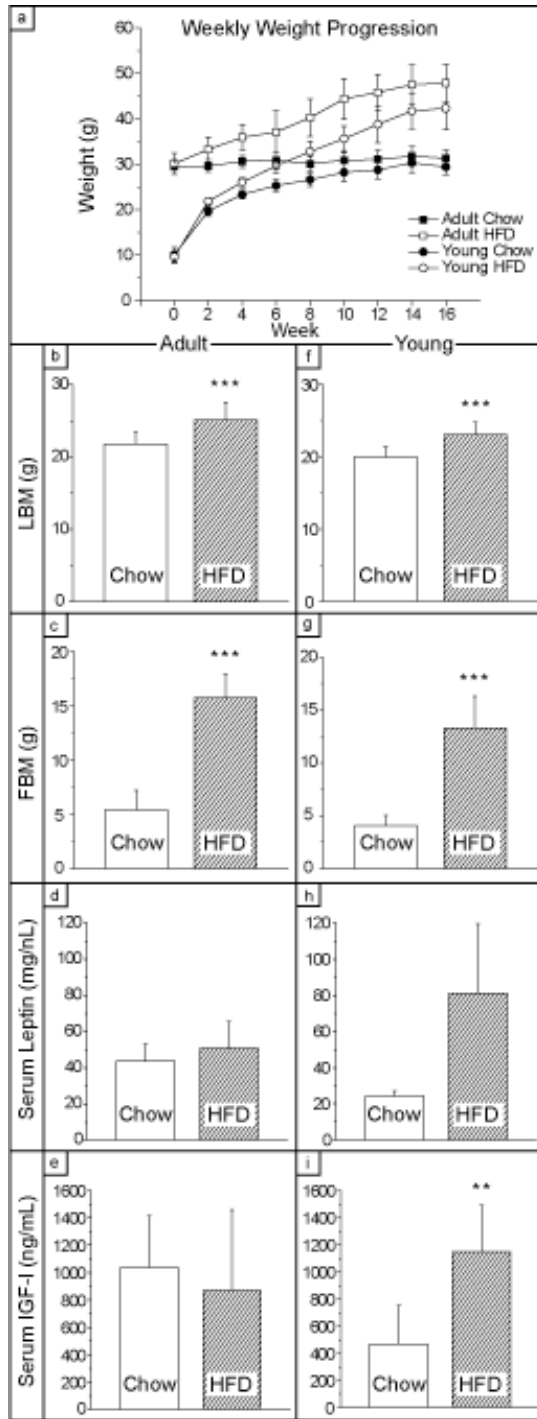
There was a 16% increase in aHFD vs aChow serum leptin concentration and a 235% increase in yHFD vs. yChow. Although not significant, the increasing trend in serum leptin concentration is in agreement with prior studies which show serum levels of leptin to increase with obesity.

IGF-I increased significantly for the yHFD group only, with a 145% increase in IGF-I concentration ( $P < 0.01$ ). As increased IGF-I is associated with increased bone size, especially at the periosteum, these data are in agreement with bone size trends observed as well as calcein findings which point to increasing bone size in young and periosteal activity in young, respectively. The lack of change in IGF-I for adults is also in agreement with the little change in bone size and the calcein finding that endosteal activity is more prevalent in aHFD.

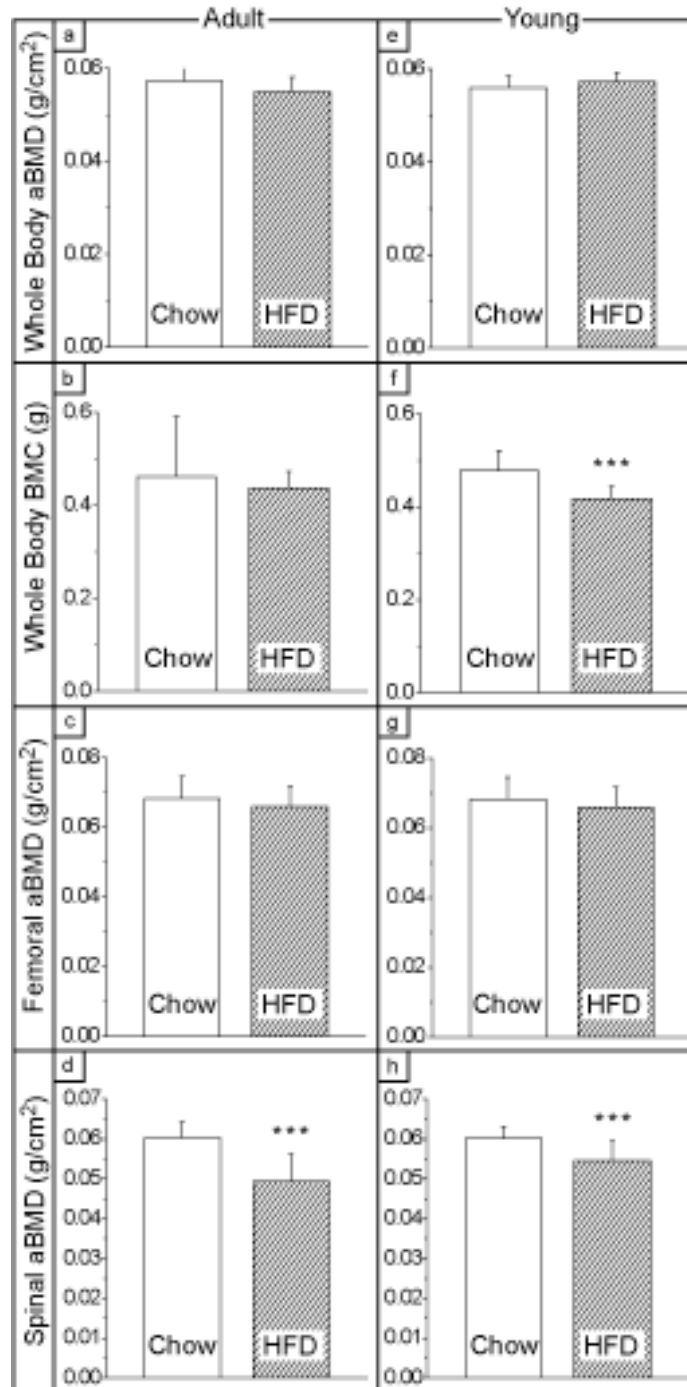
### Chapter 4.2.2 – Bone densitometry

Figure 4.2 outlines the results of bone densitometry measurements. BMC decreased 12.5% for yHFD vs. yChow, and a decreasing but non-significant trend was observed in the adult group as well. Whole-body aBMD was unaffected in both age groups, as was femoral aBMD. The only mineral measure that was highly affected was spinal aBMD, which was reduced by 18% in aHFD and 9% in yHFD compared to their Chow controls. Finally, spinal aBMD decreased significantly for both adult and young obese mice, implicating an increased spinal fracture risk. Although vertebral effects were not a part of this study, previous work by Zernicke *et al.*<sup>26</sup> found decreased L6 ash content in rats fed a high-fat-sucrose diet over 2 years. It is interesting to note that BMC decreased in the young group whereas it had increased in the past. It is likely that the reduced spinal aBMD influenced this value since we see no major changes in cortical BMD.





**Figure 4.1. Validation of Obesity Model: Body Composition, Serum Leptin Concentration, IGF-I Concentration.** (a) Average weekly weights of Chow and HFD groups. Horizontal axis is mouse age in weeks; (b) adult and (f) young lean body mass; adult (c) and (g) young fat body mass for Chow and HFD groups at conclusion of study; adult (d) and (h) young serum leptin concentration (reported in mean  $\pm$  st. err.) at conclusion of study; adult (e) and (i) young serum IGF-I concentrations at the conclusion of study. Both lean body mass and fat body mass increased, but significant increase in the fat mass and in leptin concentration for the HFD group. aChow  $n=13$ , aHFD  $n=14$ , yChow  $n=15$ , yHFD  $n=15$  (\*\*  $P<0.01$ , \*\*\*  $P<0.001$ ).



**Figure 4.2. Bone mineral.** Adult (a) and young (e) whole-body bone mineral density (aBMD) is unchanged in HFD; adult (b) and young (f) whole-body areal bone mineral content (BMC) is lower for the yHFD vs. yChow, which is likely due to the reduced spinal aBMD. Adult (c) and young (g) areal bone mineral density of the femora are unchanged; Adult (d) and young (h) areal bone mineral density of the spine are reduced for HFD despite increasing weight, leptin, and IGF-I. aChow  $n=13$ , aHFD  $n=14$ , yChow  $n=15$ , yHFD  $n=15$  (\*\*\*)  $P<0.001$ ).

### ***Chapter 4.2.3 – Bone geometry***

For measures of bone size done in the SEM, only femoral thickness in the adult group and femoral diameter in the young group are affected by high-fat diet in this study. These results are summarized in Figure 4.3. It is noted, however, that histomorphometry did point to increased cortical cross-section and perimeters, which is in agreement with the prior study (Chapter 3), as well as many other studies that find increased bone size with increasing weight, especially increasing lean body mass as we observe in this study.

### ***Chapter 4.2.4 – Bone histomorphometry measurements: cross-sectional geometry increases for both age groups while periosteal and endosteal response is different in young vs. adult.***

Endocortical single label perimeter decreased 53% in yHFD compared to the yChow group. The adult groups were unaffected. Periosteal single label perimeter increased in the Adult fat group compared to control, but this change was not statistically significant. Both of these perimeter changes point to larger bone thickness which is expected with obesity as well as increased IGF-I. There was a significant increase in endocortical area of yHFD group. An increasing non significant trend was also observed in aHFD group compared to normal. There was a significant decrease in BV/TV of yHFD vs. yChow. A decreasing non-significant trend was also observed in aHFD group compared to aChow. Although larger bone cross section is observed with the endocortical area as well as perimeter measures, the bone volume within that cross section is decreased, indicating a compensatory mechanism of size and quality.

Endocortical mineralizing surface (MS/BS) decreased with the treatment for both age groups; however, it was statistically significant only in the adult mice (MS/BS was 2.5 times higher in aHFD compared to aChow,  $P < 0.05$ ). There was a 30% decrease in endocortical bone formation rate (BFR/BS) in adult mice on fat diet. An increasing nonsignificant trend was observed in endocortical BFR/BS in yHFD vs. yChow groups.

Periosteal BFR/BS was 2.2 times higher in young fat vs. young control and 10 times higher in adult fat vs. adult control. A high standard deviation prevented these values from being statistically significant.

Endocortical and periosteal response to the treatment may be different, while the former decreases the latter may increase. Overall, endocortical BFR/BS was 3-4 higher in adult mice over the young animals whereas periosteal BFR/BS was significantly higher in young groups. These results imply that bone response changes with age; the response seems to be most focused in the periosteal region in young age but that response shifts to the endocortex with age. For both age groups, MAR did not show a response to diet.

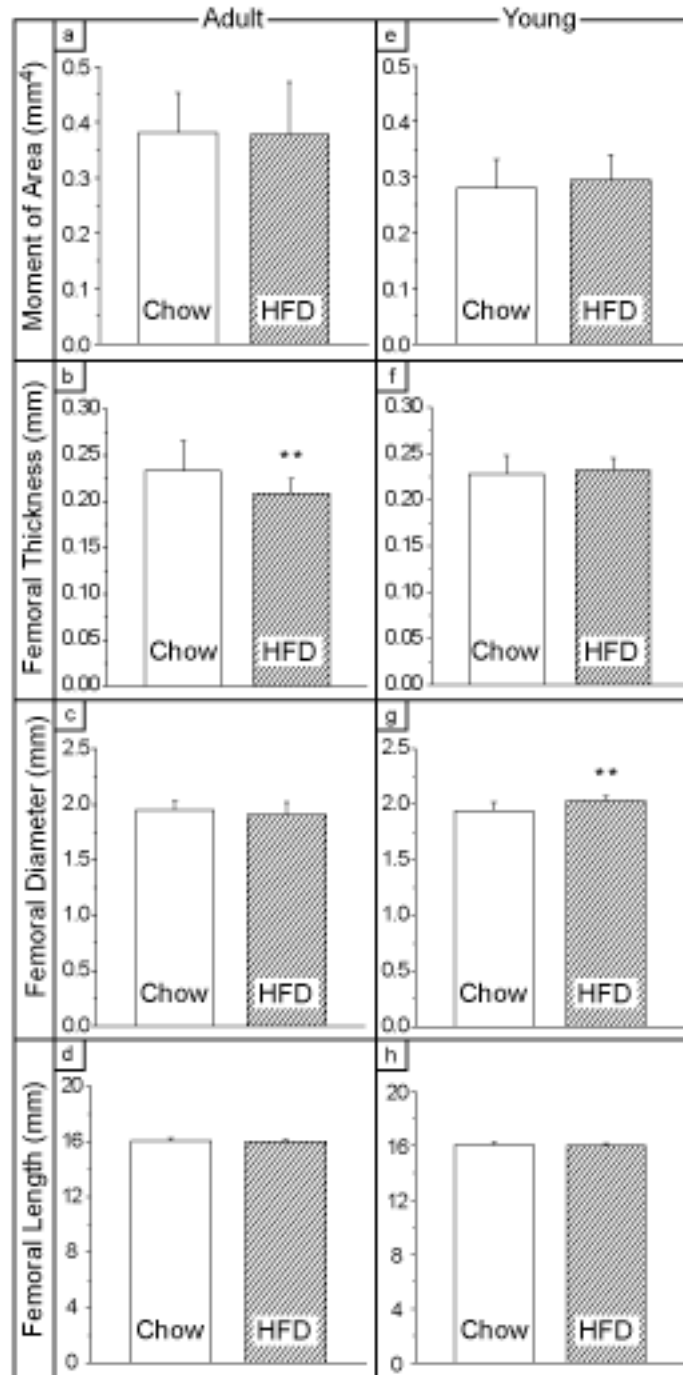


**Figure 4.3. Cortical bone size.** Adult (a) and young (e) moment of area at the dyaphysis is unchanged in HFD; adult (b) and young (f) cortical thickness is reduced in adults. Adult (c) and young (g) femoral diameters are increased in yHFD vs. yChow; Adult (d) and young (h) femoral lengths are unchanged. The general trend, although not significant points to decreasing bone size in adults and increasing bone size in young obese mice compared to Chow. aChow  $n=13$ , aHFD  $n=14$ , yChow  $n=15$ , yHFD  $n=15$  (\*\* $P<0.01$ ).

#### ***Chapter 4.2.5 – Non-enzymatic glycation shows increase of AGEs with obesity.***

Non-enzymatic glycation measurements were taken to assess the extent of advanced glycation end-products in the decalcified cortex of HFD and Chow groups. AGEs show a 31% increase in aHFD ( $42.8 \pm 7.6$  ng Quinine / mg collagen) vs. aChow ( $56.1 \pm 9.2$  ng/mg,  $P < 0.001$ ) and a 6% increase in yHFD vs. yChow ( $41.3 \pm 5.5$  ng/mg vs.  $39.1 \pm 8.7$  ng/mg, respectively,  $P > 0.05$ ). Assuming that the levels of AGEs are normal in the Chow groups, then the elevated levels in the HFD groups could help explain reduced fracture resistance, especially in the adult group which had a significant drop in fracture toughness (see next section).

#### ***Chapter 4.2.6 – Mechanical testing: Mechanical properties decrease with obesity***

Overall, a reduction of mechanical properties is observed with obesity in both young and adult groups. These results are summarized in Figure 4.4. Yield strength is 9% less in adults, 17% less in young ( $P < 0.01$ ); maximum strength is 15% less in adults ( $P < 0.05$ ) and 26% less in young ( $P < 0.01$ ). Bending modulus is 18% less in adults and 32% less in young ( $P < 0.01$ ). Fracture toughness,  $K_{Ic}$ , is 21% less in adults ( $P < 0.05$ ) but unchanged in young (8% higher, not significant). Finally, maximum load is 22% less in adult ( $P < 0.01$ ), 12.5% less in young ( $P < 0.05$ ). These results indicate a profound reduction in mechanical quality and performance with obesity.

#### ***Chapter 4.2.7 – Structural characterization: mineral organization and lamellar alignment of cortical bone is reduced in obese mice***

SEM was performed on cross-sections of femora near the fracture surface to evaluate lamellar-level structural changes. Changes in structure were most apparent at the posterior site (Fig. 4.5). In both the young and adult groups, the HFD bone showed marked areas of lamellar disorganization, whereas a similar area in the Chow appeared well-ordered.

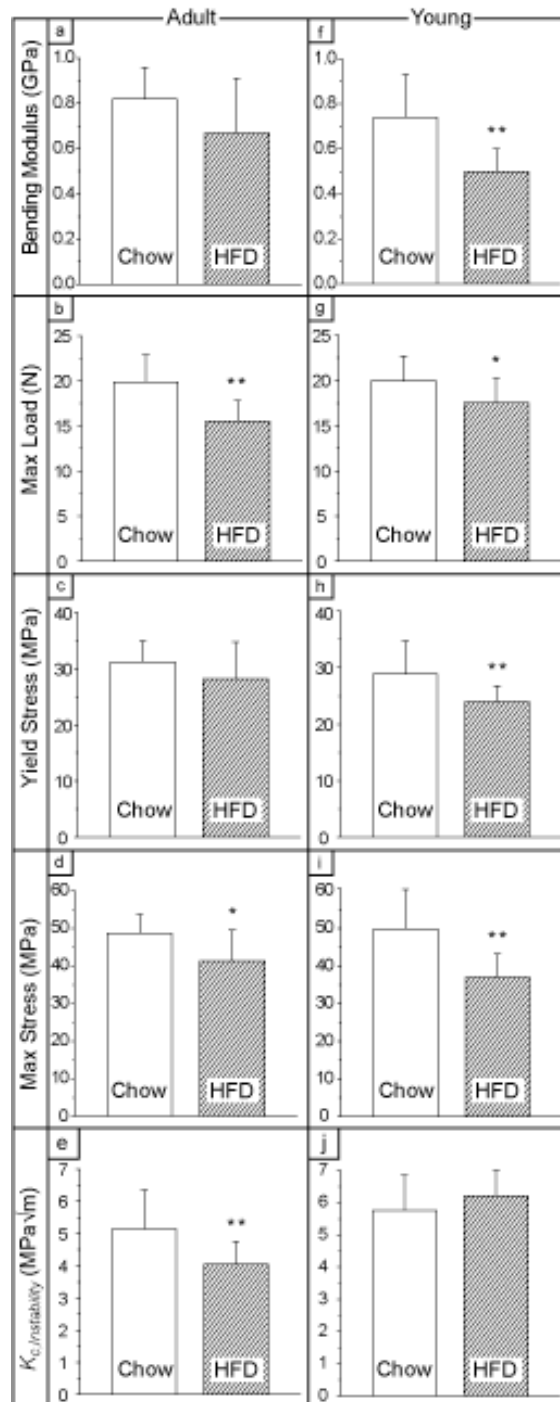


**Figure 4.4. Cortical bone quality: whole-bone and tissue-level mechanical property measurements.** Adult (a) and young (f) bending modulus; adult (b) and young (g) maximum load; adult (c) and young (h) yield stress; adult (d) and young (i) max stress; adult (e) and young (j) fracture toughness. Measured size-independent mechanical properties were significantly decreased for HFD group vs. Chow groups despite (modulus, yield and max stress, and fracture toughness); these parameters are an indication of bone-tissue quality. Size-dependent measures which address whole-bone behavior (specifically, load) also declined for HFD at both ages, likely due in part to modest bone size changes, as bone size was not able to compensate for poor mechanical quality. aChow  $n=13$ , aHFD  $n=14$ , yChow  $n=15$ , yHFD  $n=15$  (\*  $P<0.05$ ; \*\*  $P<0.01$ ).

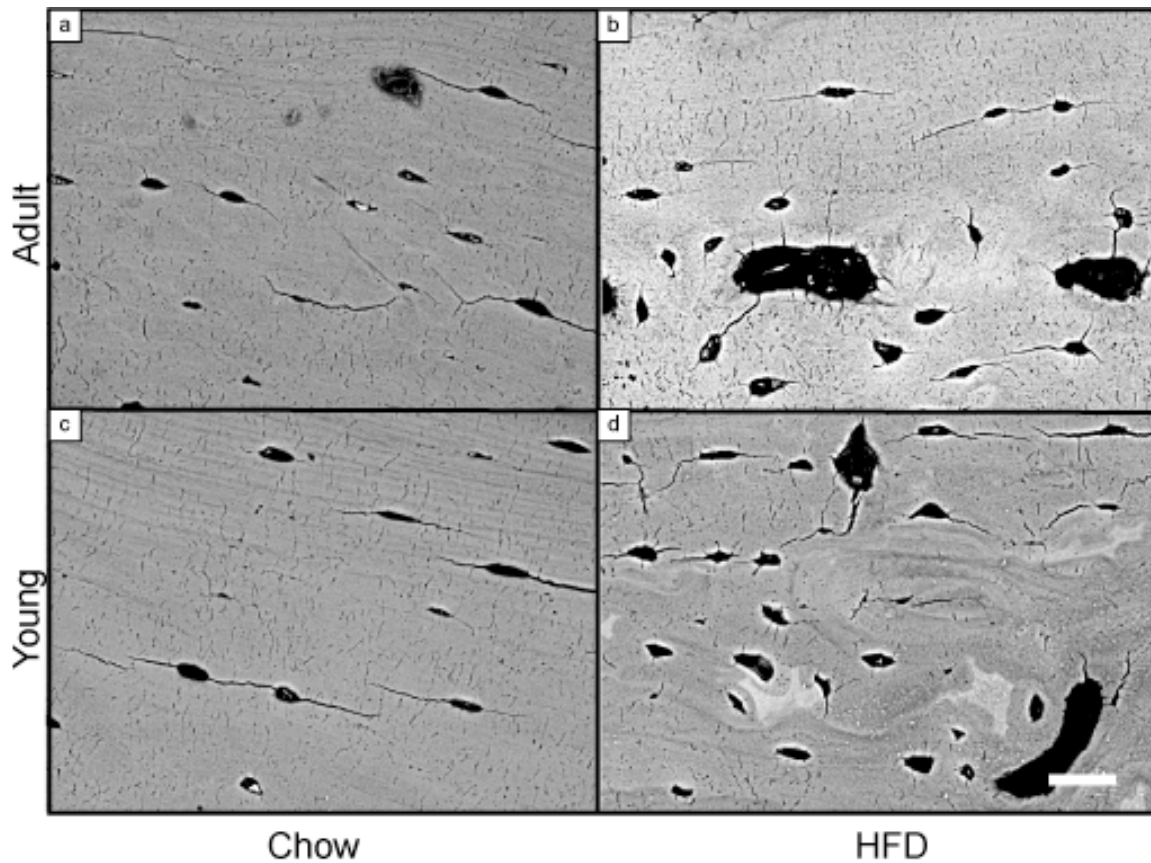


**Figure 4.5.** SEM images of of fracture region showing tissue structure changes at the posterior region. (a) aChow group; (b) aHFD; (c) yChow; (d) yHFD. The scale bar indicates 20  $\mu\text{m}$ . The posterior cortex in HFD bone (b) and (d) shows reduced alignment of osteocyte lacunae and reduction in lamellar alignment at the tissue level. These images are representative of three samples each of aHFD, yHFD, aChow, and yChow. Medial, lateral, and anterior portions of the bone sections appeared similar for HFD and Chow in both age groups.

#### ***Chapter 4.2.8 – Correlation Analysis***

In order to evaluate relationships between bone size, mechanical properties, and body composition, correlation analyses were performed between scores for each measure; correlation coefficients and corresponding *P*-values are summarized in Table 2 (Q-Q analysis revealed that the data were normally distributed). In aChow, yChow, aHFD, and yHFD groups, bone-size measures have the highest (negative) correlation coefficients with size-independent mechanical measures, although significance was more difficult to achieve in the HFD groups. The next highest predictor of mechanical properties appears to be LBM, which is not surprising as bone size is highly positively correlated with LBM. FBM is weakly negatively correlated with bone size measures, and therefore appears to have little effect on mechanical properties. BMC affected mechanical properties more so than aBMD, but as aBMD is confounded with bone size, its effects may be washed out and a more robust measure of bone mineral density, such as volumetric bone mineral density may show more strong prediction of properties.

Predictors	a. Adult Chow (n=13 <sup>†</sup> )			b. Adult HFD (n=14)		
	Size – independent measures		Size – dependent measures	Size – independent measures		Size – dependent measures
	( $\sigma_y, \sigma_w, E$ )	$K_c$	$P_u$	( $\sigma_y, \sigma_w, E$ )	$K_c$	$P_u$
aBMD	0.0808	0.2741	0.0574	-0.4976	0.2376	-0.2333
BMC	-0.1709	0.1131	0.3577	-0.4312	-0.0746	-0.0991
(D, t, M.A.)	-0.5559 *	0.3858	0.7536*	-0.5046	-0.3889	0.4426
LBM	0.1485	0.3775	0.5138	-0.2061	-0.1537	0.6519*
FBM	-0.1075	0.0715	-0.4535	-0.1394	-0.3774	-0.0796
	c. Bone size in Chow- (D, t, M.A.)			d. Bone size in HFD - (D, t, M.A.)		
LBM	0.4587			0.6377*		
FBM	-0.1284			-0.0023		
Predictors	e. Young Chow (n=15)			f. Young HFD (n=15)		
	Size – independent measures		Size – dependent measures	Size – independent measures		Size – dependent measures
	( $\sigma_y, \sigma_w, E$ )	$K_c$	$P_u$	( $\sigma_y, \sigma_w, E$ )	$K_c$	$P_u$
aBMD	-0.3357	0.2225	0.3055	0.0317	0.5767*	0.5089
BMC	-0.2654	0.3362	0.4731	0.1793	0.4383	0.2907
(D, t, M.A.)	-0.7497**	0.4931	0.1384	-0.4951	0.0037	0.214
LBM	-0.4108	0.319	0.3969	-0.2584	0.0167	0.1194
FBM	0.1384	-0.2299	-0.1014	0.1582	-0.4439	-0.2404
	g. Bone size in Chow- (D, t, M.A.)			h. Bone size in HFD - (D, t, M.A.)		
LBM	0.8133***			0.4982		
FBM	-0.1433			-0.4298		

<sup>†</sup> One mouse died in week 4 of the study from fighting.

\* $P < 0.05$

\*\* $P < 0.01$

\*\*\* $P < 0.001$ .

vBMD = volumetric bone-mineral density; M.A.= second moment of area; A = Ct. cross-sectional area;  $R_o$  = outer Ct. Rd; LBM = lean body mass; FBM = fat body mass;  $\sigma_y$  = yield strength;  $\sigma_u$ = maximum strength;  $E$  = bending modulus;  $K_c$  = fracture toughness;  $P_y$ = yield load;  $P_u$ = maximum load. (M.A., A,  $R_o$ ) = composite bone size score, ( $\sigma_y, \sigma_w, E$ ) = composite strength and modulus score.

**Table 2. Correlation coefficients between standardized properties in bone from (a)-(d) adult and (e)-(h) young groups.** Coefficients from correlation analysis applied between standardized mechanical properties and standardized bone and physiological properties of (a), (c) adult Chow group; (b), (d) adult HFD group; (e), (g) young Chow group; (f), (h) young HFD group. In cases where measurements were related and highly positively correlated, a composite score was used in the analysis. Bone size is the largest predictor of mechanical properties, more so than bone-mineral measures or body composition. Interestingly, size-independent measures of bone quality are most affected by the size of the bone, which implies a reduced quality with increasing quantity. Correlation coefficients between body mass measures and bone size measures show that LBM is positively correlated with bone size in both groups (c), (d), (g), (h) and that FBM is very weakly negatively correlated with bone size.



### Chapter 4.3 – Discussion of Adult versus Young Mouse Results

In studying the effects of obesity on bone, there is a large reduction in cortical mechanical properties in both young and adult mouse groups. Although increased bone size is expected, especially with increasing lean body mass,<sup>28,29,30,31,32,33,34</sup> the bone cannot overcome the greater forces of reduced health, *i.e.* high leptin and IGF-I levels, as well as greatly increased fat body mass. Reduced mechanical performance is also echoed in the high blood glucose levels, where fracture rates would be expected increase compared to normal controls.<sup>41,42</sup>

Calcein labeling indicates a reduction of bone quality *vs.* increasing quantity of bone with obesity, as indicated by decreasing BV/TV while geometric measures point to larger bone (increased cortical area, increasing periosteal perimeter, and decreasing endocortical perimeter). This is further supported by SEM which shows reduced tissue organization at the micro- and nano-scale. SEM shows reduced alignment of lamellae, especially in the posterior quadrant. Both these observations imply that the bone would be less able to perform its load-bearing function, which is supported by large decreases in both the size-dependent and size-independent mechanical measures (maximum load and strength/toughness, respectively).

The change in response to obesity with age is especially interesting to consider as clinical observations of fracture incidence point to a shift with increasing age. The direct effect of aging would be best investigated by starting with a large group and removing a prescribed number of animals at regular intervals throughout the study to see the progression of mechanical properties, bone mineral and size with age. To maintain a large *n* and to see if there is an overall trend worth investigating, this study serves as a starting point to future investigation, whereby the two groups are considered separately and to gauge the effects at the two ends of the age spectrum. Further study would show how the ends are connected, *i.e.* whether by a straight line or by some form of acceleration. Although the evolution of fracture risk with progressing time is not directly considered, changes are observed in cortical response to obesity in adulthood versus adolescence. The location of bone response seems to shift from the periosteal to the endocortical surface, as indicated by the calcein labeling experiment. Additionally, a minor decreasing bone size trend shows up in the adults whereas the bone size measures trend up for young animals. Both of these observations are further supported by increased serum IGF-I concentrations in young mice only. Although not significant, it is possible that age decreases the ability of bones to increase in size in response to increasing obesity. Coupled with decreasing mechanical properties, adults seem to be just as at risk for bone fracture, if not more so, than the young group. Since there is greatly increased blood glucose levels in this study, the potential diabetic state likely interferes with the body's tendency to increase bone size in response to increasing leptin, IGF-I, and body weight as would otherwise be expected. This is in agreement with Garris *et al.* who found reduced hind limb bone maturation in db/db (diabetic) and ob/ob (obese) mice was stunted compared to controls.<sup>87</sup> The prior study (Chapter 3) found a smaller effect in blood glucose levels over a longer period of time (19 weeks), and also a much larger effect in bone size (markedly increased cortical bone parameters). It is therefore highly likely that the differences in the two studies (*i.e.*, reduced effect in bone

size, whereby cortical size parameters seem to be relatively unchanged by obesity in this work) stems from the additional burden of diabetes. Studying mouse models that are less susceptible to hyperglycemia may show larger effects in the bone size such as those observed in non-diabetic humans.

Overall there is a marked reduction in mechanical performance of cortical bone in both adults as well as adolescents with obesity. This reduction is accompanied by a shift of cortical bone response from the periosteal region in young mice to the endocortical region in adult mice. Although observed fracture rates change in humans with increasing age, obesity may not be as protective against fracture as commonly thought. Factors such as hormone levels and blood glucose levels dramatically influence the effects, and may even cancel out the compensatory mechanisms such as the tendency of bone to increase its size in response to increasing body size.

## **Chapter 5 – Summary and Future Work**

### **Chapter 5.1 – Summary of findings**

#### ***Chapter 5.1.1 – Summary of Chapter 1***

Chapter 1 outlined the need for investigation of cortical bone response to obesity. With rising obesity rates, it is important to understand the implications of obesity on the daily lives of individuals. Namely, fracture risk in adolescents and adults was discussed, and the changing fracture rates with age. Specifically, children are observed to have increased fracture risk whereas adults are observed to have declining fracture risk with obesity. Factors such as hormones and diseases like diabetes have profound implications for the response of bone to adiposity. Prior work in the field was discussed, which found predominantly increasing bone size and decreasing mechanical properties.

#### ***Chapter 5.1.2 – Summary of Chapter 2***

A multitude of methods were employed in the study of the effects of obesity on cortical bone. Predominantly, bone quantity (bone size, amount of bone mineral) and bone quality (mechanical performance as well as cortical structure) were assessed using a multitude methods, namely several types of microscopy, DXA, calcein labeling, various mechanical testing techniques, and non-enzymatic glycation. Hormone levels were also evaluated to further understand the connection between fat cells and bone response.

#### ***Chapter 5.1.3 – Summary of Chapter 3***

The effect of obesity on cortical bone was evaluated in young mice only in the first study. This study has shown that diet-induced obesity in mice increases bone size yet decreases the (size-independent) mechanical properties of cortical bone. The maximum loads that the bones can sustain, however, remain essentially unchanged with the implication that the quality and quantity of bone act in a compensatory manner to optimize the load-bearing behavior of bone.

#### ***Chapter 5.1.4 – Summary of Chapter 4***

Changes in fracture risk with age inspired a follow-up study where a young group was compared to an adult group. Overall a marked reduction was observed in mechanical performance of cortical bone in both adults as well as adolescents with obesity. This reduction is accompanied by a shift of cortical bone response from the periosteal region in young mice to the endocortical region in adult mice. Although

observed fracture rates change in humans with increasing age, obesity may not be as protective against fracture as commonly thought. Factors such as hormone levels and blood glucose levels dramatically influence the effects, and may even cancel out the compensatory mechanisms such as the tendency of bone to increase its size in response to increasing body size.

## **Chapter 5.2 – Directions for Future Work**

Many questions remain regarding the response of cortical bone to obesity. One major question to be answered is how bone response progresses with age. A study to evaluate this may start with a large cohort of animals, and remove a set number at specified intervals (say, every 2 weeks). Then, measurement of mechanical properties with concurrent investigation of bone structure, calcein labeling, and NEG experiments may elucidate how bone response progresses with age.

A second question worth pursuing is an animal model closer to the human biology. Mice are easily studied in a laboratory for a variety of reasons including short lifetime, ease of handling, and affordability. To better understand human fracture risk, one might consider conducting a similar investigation to this one, but in primates or larger animals such as pigs.

A third consideration is disease. Diabetes is highly associated with obesity, and a more methodical study of its independent effects on bone fracture risk would be interesting. Specifically, obese and nonobese diabetics could be investigated, or if mouse studies are advantageous, consideration of different mouse strains such as hyperglycemia-resistant strains compared to strains which become diabetic easily would go a long way toward explaining how that specific disease can impact fracture risk.

Finally, as treatments for obesity become more prevalent, investigating how these affect fracture risk is of great importance, especially in older adults where fracture risk is already high.

For all these investigations, high levels of collaboration between various experts is imperative. Materials scientists, biologists, doctors, and microscopists have the ability to contribute in much greater capacity together than the sum of their parts might. As science becomes more and more collaborative, medical and scientific advances can occur at higher and higher rates.

## APPENDIX A – Diet Formulation

### A.1 – Control Chow for Young Study:

# PicoLab® Mouse Diet 20

# 5058\*

---

**DESCRIPTION**  
PicoLab® Mouse Diet 20 is a Constant Nutrition® formulation providing 20% protein for mouse colonies that require extra levels of energy needed for maximum production in post-partum breeding. Irradiation treatment and special 4-ply packaging provide virtually bacteria-free dietary control.

**Features and Benefits**

- Formulated with 20% protein for mouse breeding colonies
- Precision processing and selection of highest quality ingredients assures Constant Nutrition® quality
- Designed to meet the energy needs of breeding mouse colonies, transgenic strains, and mice exposed to higher stress levels
- Irradiation gives reliable microbial control and eliminates the need for autoclaving

**Product Forms Available**

- Oval pellet, 10 mm x 16 mm x 25 mm length (3/8"x5/8"x1")
- Meal (ground pellets), special order

**Other Versions Available**

- 5062 Pico-Vac® Mouse Diet 20

**CHEMICAL COMPOSITION<sup>1</sup>**

**Nutrients<sup>2</sup>**

Protein, %	.21.8	Sulfur, %	.0.27
Arginine, %	.1.15	Sodium, %	.0.25
Cystine, %	.0.31	Chlorine, %	.0.42
Glycine, %	.0.93	Fluorine, ppm	.12
Histidine, %	.0.50	Iron, ppm	.200
Isoleucine, %	.1.02	Zinc, ppm	.120
Leucine, %	.1.82	Manganese, ppm	.120
Lysine, %	.1.13	Copper, ppm	.17
Methionine, %	.0.67	Cobalt, ppm	.0.55
Phenylalanine, %	.0.97	Iodine, ppm	.1.5
Tyrosine, %	.0.64	Chromium, ppm	.0.56
Threonine, %	.0.79	Selenium, ppm	.0.30
Tryptophan, %	.0.25		
Valine, %	.1.03	<b>Vitamins</b>	
Serine, %	.1.07	Carotene, ppm	.Trace
Aspartic Acid, %	.2.13	Vitamin K (as menadione), ppm	.3.1
Glutamic Acid, %	.4.47	Thiamin Hydrochloride, ppm	.15
Alanine, %	.1.34	Riboflavin, ppm	.8.0
Proline, %	.1.54	Niacin, ppm	.90
Taurine, %	.0.02	Pantothenic Acid, ppm	.21
<b>Fat (other extract), %</b>	<b>.9.0</b>	Choline Chloride, ppm	.2200
<b>Fat (acid hydrolysis), %</b>	<b>.9.1</b>	Folic Acid, ppm	.2.9
Cholesterol, ppm	.200	Pyridoxine, ppm	.9.6
Linoleic Acid, %	.2.32	Biotin, ppm	.0.30
Linolenic Acid, %	.0.21	B <sub>12</sub> , mcg/kg	.51
Arachidonic Acid, %	.0.02	Vitamin A, IU/gm	.15
Omega-3 Fatty Acids, %	.0.32	Vitamin D <sub>3</sub> (added), IU/gm	.3.3
Total Saturated Fatty Acids, %	.2.72	Vitamin E, IU/kg	.57
Total Monounsaturated		Ascorbic Acid, mg/gm	.—
Fatty Acids, %	.2.88		
<b>Fiber (Crude), %</b>	<b>.2.2</b>	<b>Calories provided by:</b>	
Neutral Detergent Fiber <sup>3</sup> , %	.10.8	Protein, %	.23.189
Acid Detergent Fiber <sup>4</sup> , %	.3.0	Fat (ether extract), %	.21.635
<b>Nitrogen-Free Extract</b>		Carbohydrates, %	.55.176
(by difference), %	.51.8		
Starch, %	.39.3	<b>*Product Code</b>	
Glucose, %	.0.16	1. Based on the latest ingredient analysis information. Since nutrient composition of natural ingredients varies, analysis will differ accordingly.	
Fructose, %	.0.16	2. Nutrients expressed as percent of ration except where otherwise indicated. Moisture content is assumed to be 10.0% for the purpose of calculations.	
Sucrose, %	.0.71	3. NDF = approximately cellulose, hemicellulose and lignin.	
Lactose, %	.0.78	4. ADF = approximately cellulose and lignin.	
<b>Total Digestible Nutrients, %</b>	<b>.85.3</b>	5. Physiological Fuel Value (kcal/gm) = Sum of decimal fractions of protein, fat and carbohydrate (use Nitrogen Free Extract) x 4,9,4 kcal/gm respectively.	
<b>Gross Energy, kcal/gm</b>	<b>.4.60</b>		
<b>Physiological Fuel Value<sup>5</sup>, kcal/gm</b>	<b>.3.75</b>		
<b>Metabolizable Energy, kcal/gm</b>	<b>.3.56</b>		
<b>Minerals</b>			
Ash, %	.5.0		
Calcium, %	.0.81		
Phosphorus, %	.0.60		
Phosphorus (non-phytate), %	.0.33		
Potassium, %	.0.70		
Magnesium, %	.0.16		

**INGREDIENTS**  
Ground wheat, ground corn, dehulled soybean meal, wheat germ, fish meal, brewers dried yeast, corn gluten meal, porcine animal fat preserved with BHA, soybean oil, calcium carbonate, salt, dicalcium phosphate, monocalcium phosphate, choline chloride, menadione dimethylpyrimidinol bisulfite, DL-methionine, vitamin A acetate, cholecalciferol, pyridoxine hydrochloride, dried whey, folic acid, dl-alpha tocopheryl acetate, biotin, thiamin mononitrate, calcium pantothenate, lecithin, riboflavin, nicotinic acid, casein, vitamin B<sub>12</sub> supplement, manganous oxide, zinc oxide, ferrous carbonate, copper sulfate, zinc sulfate, calcium iodate, cobalt carbonate, sodium selenite.

**FEEDING DIRECTIONS**  
Feed ad libitum to mice. Plenty of fresh, clean water should be available to the animals at all times.  
*Note*—Adult mice will eat up to 5 grams of pelleted ration daily. Some of the larger strains may eat as much as 8 grams per day per animal. Feed should be available on a free choice basis in wire feeders above the floor of the cage.

8/15/99

**A.2 – HFD for both studies, D12450B is the control diet for the young vs. adult study:**

*Product Data*

**DIO SERIES DIETS**



*The “Original” High Fat Diets for Diet Induced Obesity*

**Formulas**

Product #	D12450B		D12451		D12492	
	gm%	kcal%	gm%	kcal%	gm%	kcal%
Protein	19.2	20	24	20	26.2	20
Carbohydrate	67.3	70	41	35	26.3	20
Fat	4.3	10	24	45	34.9	60
<b>Total kcal/gm</b>	<b>3.85</b>	<b>100</b>	<b>4.73</b>	<b>100</b>	<b>5.24</b>	<b>100</b>
Ingredient	gm	kcal	gm	kcal	gm	kcal
Casein, 80 Mesh	200	800	200	800	200	800
L-Cystine	3	12	3	12	3	12
Corn Starch	315	1260	72.8	291	0	0
Maltodextrin 10	35	140	100	400	125	500
Sucrose	350	1400	172.8	691	68.8	275.2
Cellulose, BW200	50	0	50	0	50	0
Soybean Oil	25	225	25	225	25	225
Lard*	20	180	177.5	1598	245	2205
Mineral Mix S10026	10	0	10	0	10	0
DiCalcium Phosphate	13	0	13	0	13	0
Calcium Carbonate	5.5	0	5.5	0	5.5	0
Potassium Citrate, 1 H2O	16.5	0	16.5	0	16.5	0
Vitamin Mix V10001	10	40	10	40	10	40
Choline Bitartrate	2	0	2	0	2	0
FD&C Yellow Dye #5	0.05	0				
FD&C Red Dye #40			0.05	0		
FD&C Blue Dye #1					0.05	0
<b>Total</b>	<b>1055.05</b>	<b>4057</b>	<b>858.15</b>	<b>4057</b>	<b>773.85</b>	<b>4057</b>

Formulated by E. A. Ulman, Ph.D., Research Diets, Inc., 8/26/98 and 3/11/99.

\*Typical analysis of cholesterol in lard = 0.95 mg/gram.

D12450B -  
Cholesterol (mg)/4057 kcal = 19  
Cholesterol (mg)/kg = 18  
D12451 -  
Cholesterol (mg)/4057 kcal = 168.6  
Cholesterol (mg)/kg = 196.5  
D12492 -  
Cholesterol (mg)/4057 kcal = 232.8  
Cholesterol (mg)/kg = 300.8



Research Diets, Inc.  
20 Jules Lane  
New Brunswick, NJ 08901  
Tel: 732.247.2390  
Fax: 732.247.2340  
info@researchdiets.com

Copyright © 2006 Research Diets, Inc. All rights reserved. DIO-1500

# APPENDIX B – Leptin ELISA kit

Rat / Mouse Leptin ELISA (EIA) Kit

9/14/09 9:50 AM



[home](#) | [email](#)

- Home
- Products
- Inquiries
- Ordering Info
- About Us
- Contact Us

[Mouse Leptin ELISA \(EIA\) Kit](#)

Catalog#  
90030

## Mouse Leptin ELISA Kit

### Featured Products

- Coenzyme A & Derivatives
- Ultra Sensitive Mouse Insulin ELISA Kit **NEW**
- Rat Leptin ELISA Kit **NEW**
- dNTP Solution
- Anti-Calcitonin Mono
- Nucleotides

Please [contact us](#) for more info...

**Sample Size :** 5µl  
Serum, plasma, or fluid

**Samples:**

**Tests:** < 96 wells (8 wells x 12 modules)

**Reagents:** In liquid form (except standard)

**Assay Range:** 0.2 - 12.8 ng/ml

**Assay Time:** Overnight procedure

**Precision:** Intra-assay precision CV ≤ 10.0%  
Inter-assay precision CV ≤ 10.0%

[CLICK FOR SUMMARY OF ASSAY](#)

[CLICK FOR RELATED PRODUCTS](#)

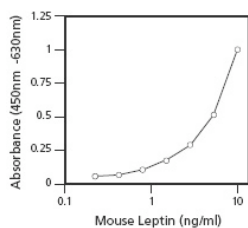
**Recovery:** When mouse leptin was spiked into mouse serum, the recovery of mouse leptin was 100% ± 20%

### Specificity:

Substance	Reactivity
r-Mouse Leptin	100%
r-Rat Leptin	100%*
r-Human Leptin	40%*
Mouse Insulin	Not detected
Rat C-Peptide	Not detected
Rat pancreatic polypeptide	Not detected
Glucagon (1-37)	Not detected
Glucagon (1-29)	Not detected
r-Human Insulin like growth factor-I	Not detected
r-Human Insulin like growth factor-II	Not detected
Human Somatostatin	Not detected

\*Can vary from lot to lot. Specific cross reactivity data is included with each kit

### Typical Standard Curve:

**Highlights:****Small Sample Volume:** Only 5µl**High Sensitivity:** 200 pg/ml using 5µl sample**Precision:** Intra-assay and inter-assay precision CV ≤ 10.0%

## Summary of Assay

### Mouse Leptin ELISA Kit (Catalog# 90030)





## APPENDIX C – IGF-I ELISA kit

Growth

# Rat/Mouse Insulin-like Growth Factor-I (IGF-I) ELISA



The IDS Rat/Mouse IGF-I kit is a two-site ELISA for the quantitative determination of IGF-I in Rat or Mouse serum or plasma. The assay uses a highly specific monoclonal "capture" antibody in microtiter wells and a high affinity polyclonal antibody labelled with horseradish peroxidase. A simple sample pre-treatment replaces acid/ethanol extraction to allow for the direct immunoassay of IGF-I, the whole process being completed within 4 hours.

### Features and Benefits

- CO-SPECIFIC for both rat and mouse IGF-I.
- SUITABLE FOR SERUM OR PLASMA - measures IGF-I in both rat or mouse serum or plasma. Ideal for research studies.
- SMALL SAMPLE VOLUME - 10 µL or 25 µL sample volume.
- IDEAL SPECIFICITY CHARACTERISTICS - no cross-reactivity with IGF-II or human IGF-I.
- NON-ISOTOPIIC 2-SITE ELISA - confers excellent specificity for IGF-I, eliminates interference.
- SIMPLE PRE-TREATMENT replaces tedious precipitation or extraction/purification procedures.



### Performance Characteristics

Code:	AC-18F1
Intended Use:	For Research Use Only
Format:	96 Wells
Methodology:	ELISA
Number of Tests per Kit:	40 determinations in duplicate
Standards:	6
Controls:	2
Specimen Type:	Serum or plasma
Specimen Volume:	25 µL (or 10 µL)
Sample Pretreatment:	Yes
Min. Det. Concentration:	<63 ng/mL
Specificity:	Rat & Mouse IGF-I 100% Rat IGF-II not detectable Human IGF-I not detectable
Assay Range:	Approx. 250-4000 ng/mL
Precision:	
CV's within run	<9%
CV's between runs	<9%
Total Assay Time:	4 Hours
Hands-on Time:	45 Minutes
Data Reduction:	4 PL fit
Wavelength:	450nm

Description	Code	Size
Rat/Mouse IGF-I ELISA	AC-18F1	96 Wells

### Contact Details

**United Kingdom:** Immunodiagnostic Systems Limited (IDS Ltd)  
10 Didcot Way, Boldon Business Park,  
Boldon, Tyne & Wear, NE35 9PD, UK  
Tel: +44 (0) 191 519 0660 Fax: +44 (0) 191 519 0760  
Email: info.uk@idsplc.com www.idsplc.com

**United States of America:** Immunodiagnostic Systems Inc (IDS Inc)  
P.O. Box 17063, Fountain Hills, AZ 85269-7063, USA  
Tel: 480 836 7435 Fax: 480 836 7437  
Email: info.us@idsplc.com www.idsplc.com

**Germany:** Immunodiagnostic Systems GmbH (IDS GmbH)  
Mainzer Landstrasse 49, 60329, Frankfurt am Main, Germany  
Tel: +49 (0) 69 3085 5025 Fax: +49 (0) 69 3085 5125  
Email: info.de@idsplc.com www.idsplc.com

**France:** Immunodiagnostic Systems EURL (IDS EURL)  
55 Rue Sainte Anne, 75002 PARIS, France  
Tél: +33 (0)1 42 44 12 63 Fax: +33 (0)1 42 44 40 76  
Email: info.fr@idsplc.com www.idsplc.com

**Scandinavia:** Immunodiagnostic Systems Nordic a/s (IDS Nordic a/s)  
Marielundvej 30, 2. Sal, 2730 Herlev, Denmark  
Tel: +45 44 84 0091 Fax: +45 44 84 0092  
Email: info.nordic@idsplc.com www.idsplc.com

AC-18FL  
Issue: 5  
Date: 15.05.09

Visit [www.idsplc.com](http://www.idsplc.com) for an extended range of products

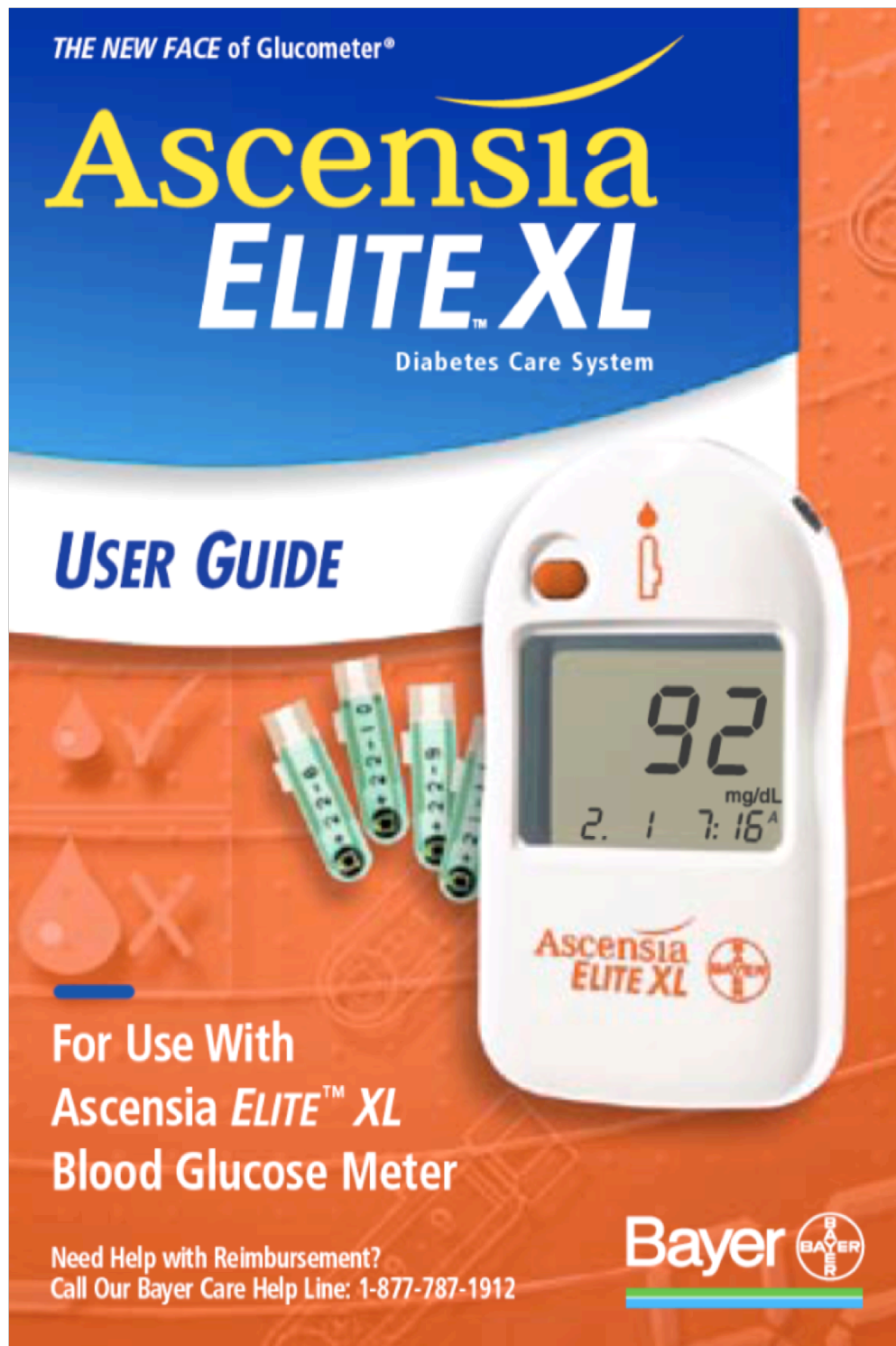
APPENDIX D – Blood Glucose Meter

THE NEW FACE of Glucometer®

# Ascensia ELITE™ XL

Diabetes Care System


## USER GUIDE



The image shows the Ascensia ELITE XL Blood Glucose Meter, a white handheld device with a digital display. The display shows a reading of 92 mg/dL, with a time of 2:17:16 and a superscript A. To the left of the meter are several green and white test strips. The meter has a small orange light and a test strip insertion slot at the top. The Bayer logo is visible on the bottom right of the meter.

For Use With  
Ascensia *ELITE™ XL*  
Blood Glucose Meter

Need Help with Reimbursement?  
Call Our Bayer Care Help Line: 1-877-787-1912

**Bayer** 

# 14 SECTION Specifications

**Test Sample:** Whole blood

**Test Result:** Plasma/serum glucose

## Reaction Chamber

**Sample Volume:** 2  $\mu$ L

**Measuring Range:** 20–600 mg/dL  
(1.1–33.3 mmol/L)

**Measuring Time:** 30 Seconds

**Calibration Curve:** Selected by use of the Code Strip

**Memory Feature:** Stores last 120 test results

## Temperature

**Compensation:** Automatic compensation with built-in thermistor

**Battery Type:** 3-volt lithium batteries  
(DL or CR2032) – 2

**Battery Life:** Approximately 1000 Tests  
(1 year of average use)

## Operating

**Temperature Range:** 50°–104° F (10°–40° C)

**Humidity:** 20–80% RH

**Dimensions:** 97.8 x 56 x 14.5 mm  
(3<sup>7</sup>/<sub>8</sub> x 2<sup>3</sup>/<sub>16</sub> x <sup>9</sup>/<sub>16</sub> in.)

**Weight:** Approximately 60g  
(2.1 ounces)

**Alarm:** “Beeps” whenever a Check Strip, Code Strip or Test Strip is inserted into the Meter, when the Test Strip is filled with blood or Control Solution, and when a test result appears in the display.

### **APPENDIX E – Blood glucose results for young study (Chapter 3)**

Blood glucose levels indicate that diabetes was likely present in most of the HFD mice in the final week of the study, but was not present for the first 18 weeks out of the 19 week study. Evaluation of levels at age 15, 21, and 22 weeks indicate that only two mice had blood glucose levels above 200 mg/dL at week 21, but 10 out of 15 HFD mice were over 200 mg/dL at week 22 and one mouse had uncontrolled diabetes. The uncontrolled diabetic mouse also died a few days prior to sacrifice and was excluded from any further analysis. None of the Chow mice exhibited blood glucose levels above 200 mg/dL, so this level was taken to be a cut-off for a diabetic state in the mice. Figure 7 shows the blood glucose levels at age 15, 21, and 22 weeks, as well as the glucose tolerance test results at age 22 weeks. The mice were sacrificed two days following the glucose tolerance test, so Figure A1c-d reflects the glycemic condition of the mice at the conclusion of the study. There is a possibility that such incidence of diabetes could have had some influence on the observed data; however, as this diabetic condition presented itself very late in the study, we conclude that it is unlikely to be the sole contributor to the effects observed.

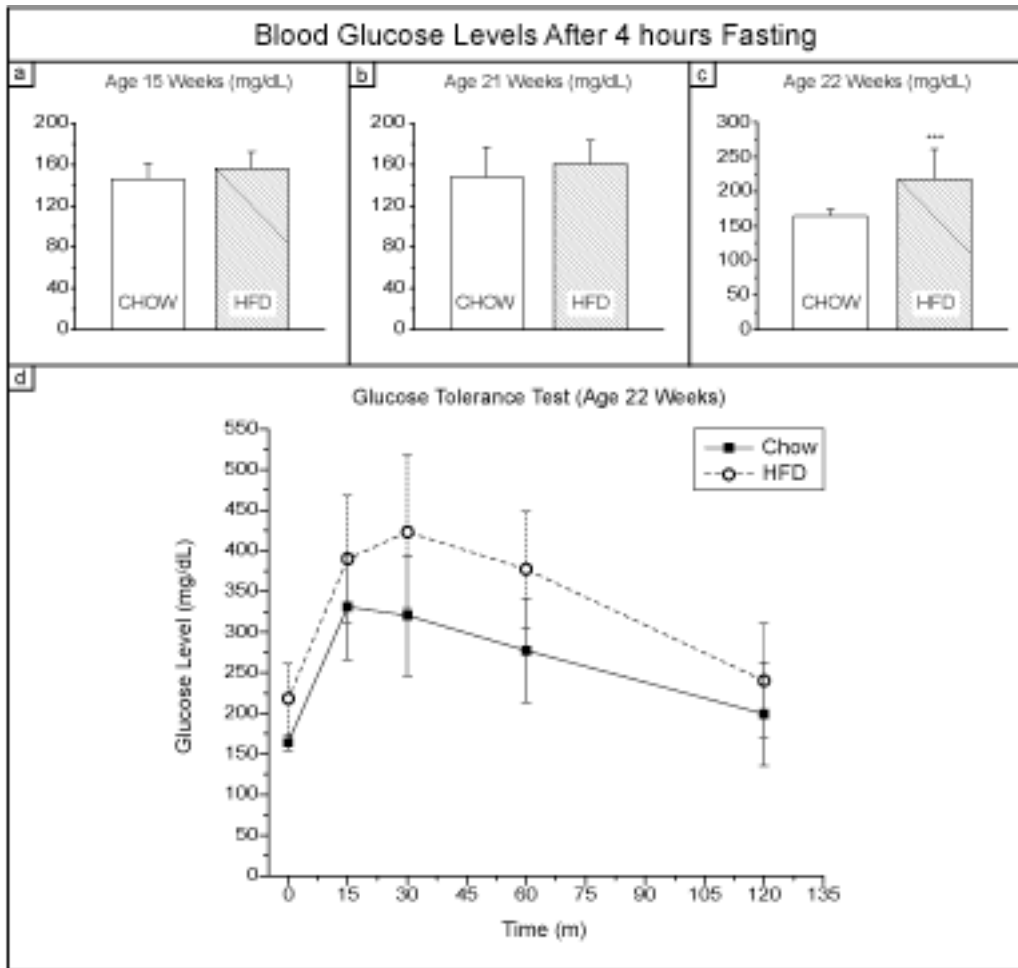


**Figure A1. Blood glucose levels after 4 hour fasting in young study.** (a) Blood glucose levels at age 15 weeks; (b) blood glucose levels at age 21 weeks; (c) baseline blood glucose levels in glucose tolerance test at age 22 weeks; (d) glucose tolerance test curve at age 22 weeks. At week 21, two HFD mice exhibited blood glucose levels over 200 mg/dL, and at week 22, 10 out of 15 HFD mice were hyperglycemic. One mouse at age 22 weeks had uncontrolled diabetes and died shortly prior to the conclusion of the study. Figure reproduced from Ref. 72.

## REFERENCES

- <sup>1</sup> K. M. Flegal, *et al.*, JAMA **288**, 1723 (2002).
- <sup>2</sup> P. G. Kopelman. Nature **404**, 635 (2000).
- <sup>3</sup> D.A. Galuska, *et al.*, Morbidity & Mortality Weekly Report **57**, 765 (2008).
- <sup>4</sup> A. A. Hedley, *et al.*, JAMA **291**, 2847 (2004).
- <sup>5</sup> S. L. Edelstein, *et al.*, Am. J. Epidemiol. **138**, 160 (1993).
- <sup>6</sup> A. M. Schott, *et al.*, Osteoporos. Int. **8**, 247 (1998).
- <sup>7</sup> H. S. Glauber, *et al.*, J. Clin. Endocrinol. Metab. **80**, 1118 (1995).
- <sup>8</sup> K. E. Ensrud, *et al.*, J. Am. Geriatr. Soc. **51**, 1740 (2003).
- <sup>9</sup> I. R. Reid, Osteoporos. Int. **19**, 595 (2008).
- <sup>10</sup> C. Albala, *et al.*, Int. J. Obesity **20**, 1027 (1996).
- <sup>11</sup> N. D. Nguyen, *et al.*, BMC Musculoskelet. Disord. **6**, 11 (2005).
- <sup>12</sup> C. De Laet, *et al.*, Osteoporos. Int. **16**, 1330 (2005).
- <sup>13</sup> E. S. Siris, *et al.*, JAMA **286**, 2815 (2001).
- <sup>14</sup> A. R. Folsom, *et al.*, Archives Internal Med **160**, 2117 (2000).
- <sup>15</sup> E. D. Taylor III, *et al.*, Pediatrics **117**, 2167 (2006).
- <sup>16</sup> A.P. Hills, *et al.*, Child Care Health Dev. **18**, 29 (1992).
- <sup>17</sup> P. Colne, *et al.*, Gait Posture **28**, 164 (2008).
- <sup>18</sup> L. Wang, *et al.*, Med. Sci. Monit. **14**, CR129 (2008).
- <sup>19</sup> A. Bener, *et al.*, J. Rheumatol. **8**, 32 (2005).
- <sup>20</sup> S. Kirchengast, *et al.*, Maturitas **39**, 133 (2001).
- <sup>21</sup> L. Vico, *et al.*, Osteoporos. Int. **2**, 153 (1992).
- <sup>22</sup> M. Wapniarz, *et al.*, J. Bone Miner. Res. **12**, 248 (1997).
- <sup>23</sup> K. J. Ellis, Physiol. Rev. **80**, 649 (2000).
- <sup>24</sup> V. Brahmabhatt V, *et al.*, Int. J. Obesity **22**, 813 (1998).
- <sup>25</sup> K. C. Li, *et al.*, Calcif. Tissue Int. **47**, 308 (1998).
- <sup>26</sup> R. F. Zernicke, *et al.*, Bone **16**, 25 (1995).
- <sup>27</sup> C. H. Turner, *et al.*, Bone **14**, 595 (1993).
- <sup>28</sup> D. B. Burr, J. Bone Miner. Res. **12**, 1547 (1997).
- <sup>29</sup> H. M. Frost, Bone **21**, 211 (1997).
- <sup>30</sup> A. Janicka, *et al.*, J. Clin. Endocrinol. Metab. **92**, 143 (2007).
- <sup>31</sup> M. A. Petit, *et al.*, Bone **35**, 750 (2004).
- <sup>32</sup> M. A. Petit, *et al.*, Bone **36**, 568 (2005).
- <sup>33</sup> S. Wu, *et al.*, Ann. Hum. Bio. **34**, 344 (2007).
- <sup>34</sup> A. Pietrobelli, *et al.*, Obesity Res. **10**, 56 (2002).
- <sup>35</sup> L. E. Lanyon, *et al.*, J. Biomechanics **17**, 897 (1984).
- <sup>36</sup> C. H. Turner, Bone **23**, 399 (1998).
- <sup>37</sup> M. Bluher, *et al.*, Science **299**, 572 (2003).
- <sup>38</sup> J. He, *et al.*, Bone **38**, 826 (2006).
- <sup>39</sup> W. W. Peppler, *et al.*, Calcif. Tissue Int. **33**, 353 (1981).
- <sup>40</sup> G. Karsenty, Cel. Metab. **4**, 341 (2006).
- <sup>41</sup> L. L. Lipscombe, *et al.*, Diabetes Care **30**, 834 (2007).
- <sup>42</sup> M. T. Saha, *et al.*, Osteoporos Int. **20**, 1401 (2009).

- 
- <sup>43</sup> D. Vashishth *et al.*, 50<sup>th</sup> ann. mtg. of the Orthopaed. Res. Soc., Poster No. 0497 (2004).
- <sup>44</sup> D. Vashishth, *et al.*, *Bone* **28**, 195 (2001).
- <sup>45</sup> A.J. Bailey, *et al.*, *Mech. Ageing Dev.* **106**, 1 (1998).
- <sup>46</sup> J. F. Woessner, *Arch. Biochem. Biophys.* **93**, 440 (1961).
- <sup>47</sup> A. M. Parfitt, *Calcif. Tissue Int.* **42**, 284 (1988).
- <sup>48</sup> J. J. Kruzic, *et al.*, *J Biomed Mater Res A* **74A**, 461 (2005).
- <sup>49</sup> M.H. Lacire, MH, *et al.*, *ASME PVP* **338**, 13 (1999).
- <sup>50</sup> Y. Takahashi, Y, *Int J Pres Ves Pip* **79**, 385 (2002).
- <sup>51</sup> P. J. Thurner, *et al.*, *Bone* (2010). In press, DOI: 10.1016/j.bone.2010.02.014.
- <sup>52</sup> R. O. Ritchie, *et al.*, *Bone* **43**, 798 (2008).
- <sup>53</sup> E399, West Conshohocken, PA: American Society for Testing and Materials; 2006.
- <sup>54</sup> R. K. Nalla, RK, *et al.*, *Biomaterials* **26**, 217 (2005).
- <sup>55</sup> K. J. Koester, *et al.*, *Nat Mater* **7**, 672 (2008).
- <sup>56</sup> A. Zahoor, *Ductile fracture handbook. I*, pp. 2-9-2-16. Palo Alto: Electric Power Research Institute; 1989.
- <sup>57</sup> Currey, JD *Bones*. Princeton: Princeton University Press; 2002.
- <sup>58</sup> P. Roschger, *et al.*, *Bone* **23**, 319 (1998).
- <sup>59</sup> Goodhew, Humphreys, & Beanland. *Electron Microscopy and Analysis*. 3<sup>rd</sup> ed. Taylor & Francis (2001).
- <sup>60</sup> M. M. Giraud-Guille, *Calcif Tissue Int* **42**, 167 (1988).
- <sup>61</sup> M. A. Rubin, *et al.*, *Bone* **35**, 11 (2004).
- <sup>62</sup> M. A. Rubin, *et al.*, *Micron* **36**, 653 (2005).
- <sup>63</sup> W. C. Oliver & G. M. Pharr, *J Mater Res* **19**, 3 (2004).
- <sup>64</sup> J. Y. Rho, *et al.*, *Bone* **25**, 295 (1999).
- <sup>65</sup> C. E. Hoffler, *et al.*, *Bone* **26**, 603 (2000).
- <sup>66</sup> S. Hengsberger, *et al.*, *Bone* **30**, 178 (2002).
- <sup>67</sup> A. J. Bushby, *et al.*, *J Mater Res* **19**, 249 (2004).
- <sup>68</sup> B. Tang, *et al.*, *J Mater Sci: Mater Med* **18**, 1875 (2007).
- <sup>69</sup> J. Vlassenbroeck, *et al.*, *Nucl Instr & Meth A* **580**, 442 (2007).
- <sup>70</sup> M.B. Leonard, *et al.*, *Am. J. Clin. Nutr.* **80**, 514 (2004).
- <sup>71</sup> M. W. Hamrick, *et al.*, *Bone* **34**, 376 (2004).
- <sup>72</sup> S. S. Ionova-Martin, *et al.*, *Bone* **46**, 217 (2010).
- <sup>73</sup> M. E. Muller, *et al.*, *Osteoporosis Int.* **14**, 345 (2003).
- <sup>74</sup> D. M. Black, *et al.*, *J. Bone Miner. Res.* **23**, 1326 (2008).
- <sup>75</sup> S. Boutroy, *et al.*, *J. Bone Miner. Res.* **23**, 392 (2008).
- <sup>76</sup> C. M. Steppan, *et al.*, *Reg. Peptides* **92**, 73 (2000).
- <sup>77</sup> P. Ducy, *et al.*, *Cell* **100**, 197 (2000).
- <sup>78</sup> J. A. Tamasi, *et al.*, *J. Bone Miner. Res.* **18**, 1605 (2003).
- <sup>79</sup> M. Lorentzon, *et al.*, *J. Bone Miner. Res.* **18**, 1871 (2006).
- <sup>80</sup> X. Wang, *et al.*, *Calcif. Tissue Int.* **80**, 374 (2007).
- <sup>81</sup> S. Lin, *et al.*, *Int. J. Obesity* **24**, 639 (2000).
- <sup>82</sup> M. Amling, *et al.*, *BioEssays* **22**, 970 (2000).
- <sup>83</sup> P. A. Baldock, *et al.*, *J. Bone Miner. Res.* **21**, 1600 (2006).
- <sup>84</sup> P. A. Baldock, *et al.*, *J. Biol. Chem.* **282**, 19092 (2007).
- <sup>85</sup> N. K. Pollock, *et al.*, *Am. J. Clin. Nutr.* **86**, 1530 (2007).

---

<sup>86</sup> E. de Margerie, *et al.*, J. Exp. Biol. **207**, 869 (2004).

<sup>87</sup> D. R. Garris, *et al.*, Diabetes Obes. and Metab. **9**, 311 (2007).